Development and evaluation of an in vitro model of exercise for studying AMPK signaling dynamics in skeletal muscle

By

Kyle D. Dumont

B.Sc., McGill University, 2016

Thesis Submitted in Partial Fulfillment of the
Requirements for the Degree of
Master of Science

in the
Department of Biomedical Physiology and Kinesiology
Faculty of Science

© Kyle Dumont 2020
SIMON FRASER UNIVERSITY
Spring 2020

Copyright in this work rests with the author. Please ensure that any reproduction or re-use is done in accordance with the relevant national copyright legislation.

Approval

Name:	**Kyle Dumont**
Degree:	**Master of Science**
Title:	**Development and evaluation of an in vitro model of exercise for studying AMPK signaling dynamics in skeletal muscle**
Examining Committee:	**Chair:** Sam Doesburg Associate Professor
	David Clarke Senior Supervisor Associate Professor
	Damon Poburko Supervisor Associate Professor
	Wade Parkhouse Supervisor Professor
	Gordon Rintoul Supervisor Associate Professor Department of Biological Sciences
	Christopher G.R. Perry External Examiner Associate Professor School of Kinesiology and Health Science, Faculty of Health, York University
Date Defended/Approved:	March 13, 2020

Abstract

Exercise promotes AMP-activated protein kinase (AMPK) signaling in skeletal muscle, where it functions to enhance the expression of fitness-promoting genes. The magnitude of the adaptations depends in part on the dynamics of AMPK signaling; however, the time course of AMPK signaling remains poorly characterized. The purpose of my thesis was to develop and evaluate electrical stimulation of cultured C_2C_{12} myotubes as a method to study AMPK signaling dynamics. I confirmed that differentiation resulted in contractile C_2C_{12} myotubes, that AMPK signaling was detectable, and that electrical stimulation increased cellular oxygen consumption. In response to three hours of electrical stimulation, AMPK signaling increased. Upon cessation of stimulation, AMPK signaling decreased. However, the magnitude of signaling was marginal, such that further work is required to define experimental conditions that lead to robust AMPK signaling. I conclude that electrical stimulation of C_2C_{12} myotubes is a promising means to study AMPK signaling dynamics.

Keywords: Exercise; AMPK; Cell Signaling; Skeletal Muscle; C2C12

Acknowledgements

I would like to express sincere gratitude towards Dr. David Clarke for giving me the opportunity to study in your lab. The rigor with which you approach science and writing is truly inspirational and I have learned a great deal because of it. Thank you very much for your guidance and support throughout my degree.

To the members of the Clarke lab, thank you for creating a positive work environment. Eli, thank you for sitting next to me for the past two years and putting up with me. TJ, thank you for all the skiing adventures and motivation to push me through my degree. Ian, thank you for supporting all my coffee breaks and scrutinizing my work every chance you could. Finally, Clare, thank you for your help setting up the lab.

This work would not have been possible without the help of several undergraduate students. To Chelsea Ribeiro (oxygen measurements; Figure 3.13 and 3.14), Katie Milligen (optimization of oxygen sensing), Jasdeep Dhanjal (differentiation; Figure 3.1 to 3.3), Sebastien Weber (optimization of western blot protocol), and Keerthana Kumar (optimization of western blot protocol and air exposure data; Figure 3.10), thank you very much for all of your help throughout my degree. Your efforts are in part what made this thesis possible.

I would like to extend a special thank you to Dr. Leanne Ramer. You have been everything from a best friend to a second mother and everything in between. Thank you for all your support and laughs you have provided throughout my degree. I am truly grateful to have you in my life.

To my friends and family who never seem to understand what I am saying when I talk about my work, thank you.

Lastly, I would like to thank the Department of Biomedical Physiology and Kinesiology at Simon Fraser University for all their help, support, and advice throughout my degree.

Table of Contents

List of Figures

Chapter 1. Background

1.1. Overview

The global rise in metabolic diseases are reaching epidemic proportions, with exercise representing an effective therapy to limit and reverse the negative health outcomes associated with these diseases [1-3]. The health benefits conferred by exercise are well established [4-7], but the molecular mechanisms by which exercise promotes health are incompletely understood. Ultimately, a better understanding of the molecular mechanisms that underpin exercise-mediated adaptations in skeletal muscle could provide improved personalized exercise interventions.

This thesis pertains to AMPK, a prototypical signaling protein that is involved in cellular energy homeostasis. Here, I discuss concepts related to cell signaling and how proteins are required for signal transduction. I then introduce AMPK and describe its control and functions as they pertain to exercise-mediated adaptations in skeletal muscle. Lastly, I introduce an in vitro approach to study AMPK signaling dynamics in skeletal muscle.

1.2. Molecular mechanisms of skeletal muscle adaptations to exercise training

Skeletal muscle is subject to various stressors during exercise such as mechanical load, hormonal and metabolic perturbations, and neuronal activation [8]. Information pertaining to the stressors is biochemically encoded by the cell and transmitted through the intracellular signaling network, which coordinates the subsequent adaptations [8, 9]. Different stressors activate different portions or subnetworks of the intracellular signaling network, with different exercise modalities exerting distinct stressors on the cells. For example, resistance exercise activates pathways associated with contractile proteins, whereas endurance exercise activates pathways associated with oxidative metabolism [8, 9]. The resulting signals are ultimately propagated to the interior of the cell where the adaptive response takes places.

Proteins are essential components of intracellular signaling networks. The biochemical mechanisms of protein signaling can be grouped into four main categories: protein-protein interactions, post-translational modifications (PTM), conformational changes, and localization [10]. Most signaling systems feature one or more of these categories of biochemical events. Src family kinases, for example, are prototypical signaling proteins that involve all four categories of biochemical events [11]. In brief, Src kinases are either active (phosphorylated at Tyr-416) or inactive (phosphorylated at Tyr-527, Figure 1.1) [11]. Activation of a Src kinase is initiated by de-phosphorylation of Tyr-527 (a PTM). Dephosphorylation de-stabilizes the protein and changes its conformation to an open state. This change in conformation increases the activity of the catalytic domain (protein-protein interaction), which causes autophosphorylation at Tyr-416 (a PTM). Phosphorylation of Tyr-416 stabilizes the kinase in an open conformation, thus promoting its ability to interact with other proteins that may cause shifts in intracellular localization [11]. Additionally, each of the previously mentioned steps provides an opportunity to control Src kinase activity.

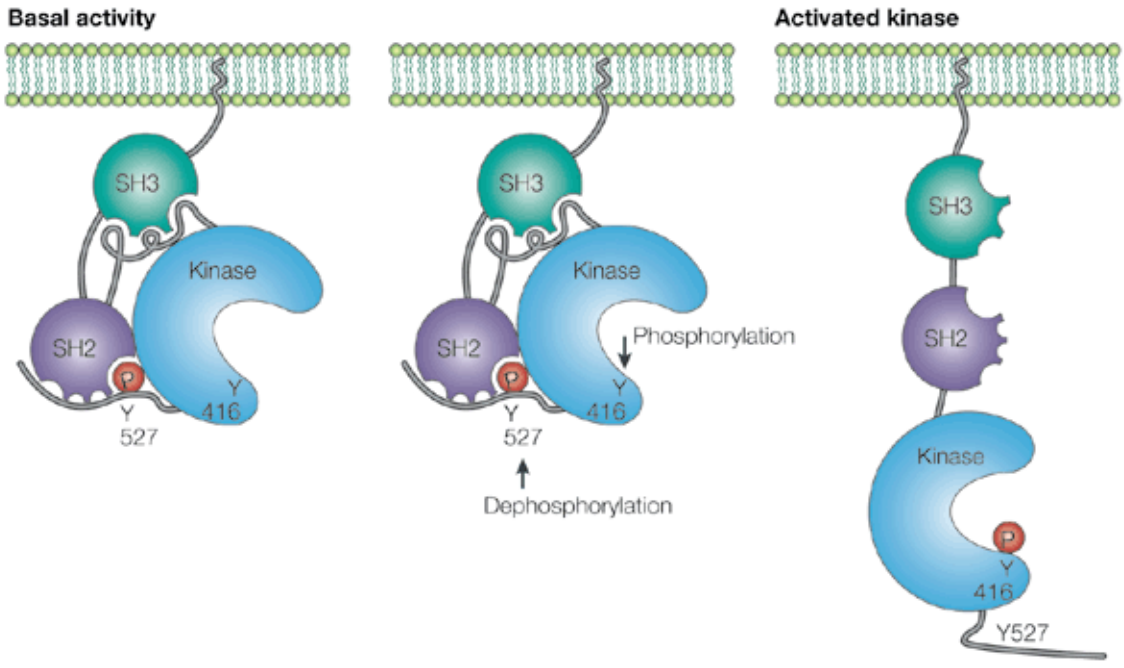

Figure 1.1 Activation of Src kinase from the inactivated (left) to the activated (right) state

Src kinase consists of three domains: the kinase domain, Src homology 2 (SH2), and Src homology 3 (SH3). The inactive state of a Src kinase (left) is characterized by Tyr-527 phosphorylation, which promotes the kinase to adopt a compact closed conformation. Dephosphorylation of Tyr-527 causes a conformational change to an open state, which increases kinase activity at the catalytic site, increasing the likelihood Tyr-416 will become phosphorylated (middle). Upon Tyr-416

phosphorylation, the Src kinase stabilizes in an open conformation, such that it more readily interacts with other proteins (right). Adapted and reprinted with permission [12].

Amongst the biochemical mechanisms described above, protein phosphorylation and allosteric activation are particularly common. Protein phosphorylation is a reversible biochemical reaction involving the transfer of a phosphoryl group from a nucleoside triphosphate [commonly adenosine triphosphate (ATP)], to a protein substrate [10], as indicated by Equation 1:

$$Protein \cdots OH + ATP \xrightarrow{Protein\ Kinase} Protein \cdots PO_4 + ADP \quad (1)$$

The transfer of a phosphoryl group to a protein substrate is catalyzed by a class of enzymes called *kinases*. Chemically, protein kinases bind the protein substrate and Mg-ATP [13]. The protein substrate and the γ-phosphate of ATP are positioned adjacent to each other [14]. A proton is removed from the phosphorylatable residue of the substrate, leaving the oxygen molecule exposed [14]. The exposed oxygen attacks the terminal phosphoryl group to form a metaphosphate intermediate. Finally, adenosine diphosphate (ADP) is displaced and the phospho-protein is formed [14]. This chemical modification can alter the function of the substrate protein in multiple ways. For example, the biological activity, stabilization, and subcellular localization of proteins can all be modified by changing the phospho-status of a protein. [10]. Overall, protein phosphorylation plays significant roles in signaling networks due to its ability to modify protein function [15].

Similar to phosphorylation, allosteric activation is involved in many aspects of protein function [16]. Allostery is a biochemical process in which effectors bind to a regulatory site other than the catalytic site, inducing a conformational change that influences the enzymatic activity [17-19]. An example of allosteric activation occurs when adenosine monophosphate (AMP, a breakdown product of ADP) binds to AMP-activated protein kinase (AMPK, described below) [20]. Binding of AMP to AMPK brings together the regulatory and the catalytic sites of AMPK and in doing so, increase the activity of the catalytic site [20, 21]. Although allosteric activation is less potent compared to phosphorylation at the regulatory site of AMPK (3-fold versus 100-fold [20, 22]), allosteric activation nonetheless plays an important role in AMPK signaling because its effects are multiplicative with those of phosphorylation [23]. Taken together, protein phosphorylation and allosteric activation are essential in transmitting intracellular signals. Below, I describe

how protein phosphorylation and allosteric activation play a fundamental role in activating and transmitting the signal of AMPK.

1.3. AMP-activated protein kinase encodes cellular energy levels

Cellular energy status is monitored by AMP-activated protein kinase (AMPK) [22, 24]. AMPK exists as a complex of three subunits: α, β, and γ [25]. Each of the three subunits exist as two or three isoforms (α1 and α2, β1 and β2, and γ1, γ2, and γ3) allowing for 12 different combinations of the AMPK heterotrimer. In human skeletal muscle, three of the possible 12 isoforms are expressed (α1β2γ1, α2β2γ1, α2β2γ3) [26]. The subunits each perform distinct functions: the α subunit contains the catalytic site and an activating phosphorylation site (Thr-172), the β subunit connects the α and γ subunits and features a carbohydrate binding site that enables AMPK to associate with glycogen, and the γ subunit features binding sites for the adenine nucleotides (ATP, ADP, and AMP).

Binding of ATP, AMP, or ADP to the γ subunit activates AMPK in the following ways [24]. First, binding of AMP and ADP to the γ subunit promotes phosphorylation of Thr-172 while simultaneously protecting this site from dephosphorylation [23, 24]. Additionally, AMP, but not ADP, allosterically activates AMPK [23]. Lastly, ATP competes with AMP and ADP for binding; binding of ATP causes no change in AMPK activity [27]. Some ATP must, however, be available to bind at the regulatory site for phosphorylation of Thr-172 to occur. If ATP is absent or the ATP binding site on the catalytic subunit is blocked, phosphorylation of Thr-172 cannot occur. If conditions conducive to phosphorylation exist, an upstream kinase (namely LKB1 or CaMKK in skeletal muscle [28]) catalyzes Thr-172 phosphorylation. Ultimately, Thr-172 phosphorylation results in AMPK activation whose effects favor a metabolic shift to maintain energy status of the cell (described below).

1.4. Exercise-mediated AMPK activity

Exercise is a potent physiological activator of AMPK in skeletal muscle because contraction markedly enhances ATP turnover by up to 100-fold [29-31]. During exercise, activated AMPK promotes catabolism and impairs anabolism through several molecular mechanisms. For example, AMPK phosphorylates acetyl-CoA carboxylase (ACC), which

impairs the cell's ability to synthesize lipids (Figure 1.2A). AMPK also enhances glucose availability by promoting the translocation of GLUT4 to the plasma membrane by phosphorylating TBC1 domain family member 1 (TBC1D1) [32, 33]. Collectively, these activities help preserve the intracellular concentration of ATP [24, 25].

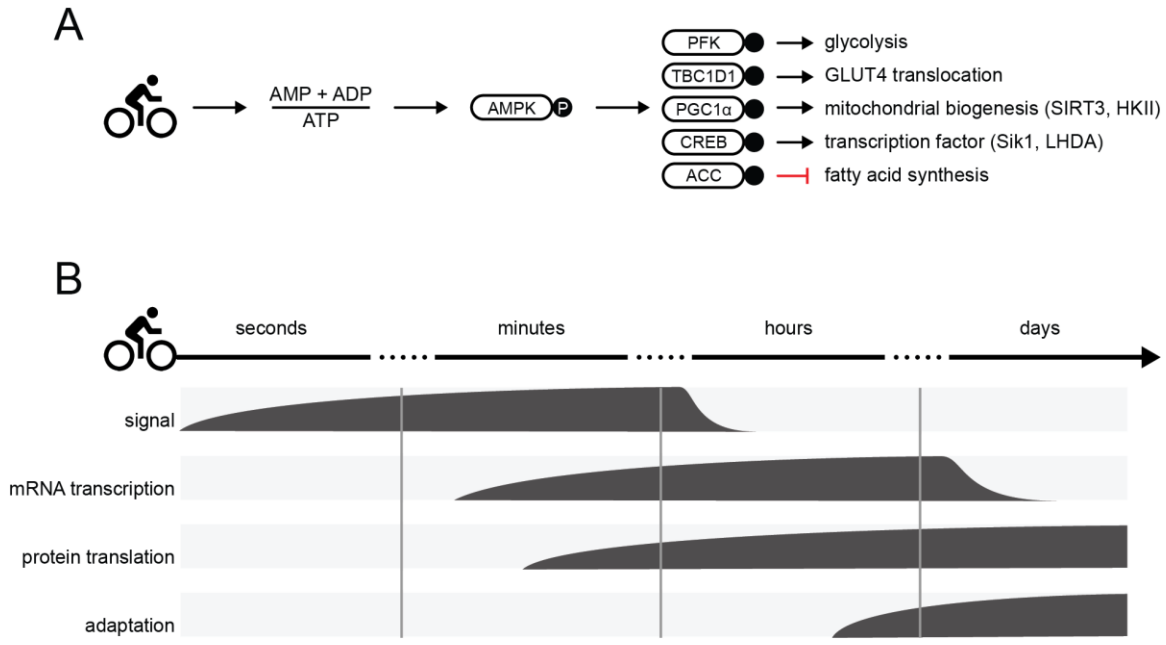

Figure 1.2 AMPK-mediated adaptations in skeletal muscle in response to exercise

(A) AMPK signaling in response to exercise. Exercise causes increased levels of AMP and ADP and decreased ATP, which leads to AMPK activation. Active AMPK phosphorylates its protein targets, which increases (black arrow) or decreases (red 'T') their activities. (B) The kinetics of molecular processes leading to exercise-mediated cellular adaptations. Exercise alters signaling, followed by mRNA transcription, and then protein translation, which ultimately lead to adaptation, i.e., changes to cellular organelles and structure, protein levels, and function.

Although AMPK is important for orchestrating immediate responses to an energy deficit, it also controls more persistent adaptations such as mitochondrial density, quality and morphology [24, 34-36]. In response to increased energy expenditure, the rate of mitochondrial biogenesis, the process of increasing mitochondrial mass, increases (Figure 1.2A) [37-39]. This process expands the mitochondrial network via a coordinated response of mitochondrial fission and upregulation of mitochondrial proteins [24]. AMPK facilitates this mitochondrial response by binding to and phosphorylating the transcriptional coactivator peroxisomal proliferator-activated receptor-γ co-activator-1α (PGC1α), which in turn is responsible for regulating mitochondrial biogenesis [37, 40-44]. Furthermore, data from β1-β2 null mice (effectively an AMPK knockout mouse) and LKB1 knockout

mice indicate a diminished mitochondrial response to exercise [30, 45-47]. Altogether, AMPK is important for coordinating mitochondrial adaption in response to exercise.

Cellular signals do not merely turn on or off, rather their activity is *dynamic*, i.e., the signal magnitudes change over time. How the dynamics of the AMPK signal orchestrates downstream adaptation is poorly understood. Signaling dynamics accounts for yet another avenue of information encoding within the cell [48, 49]. Signaling specificity is enabled by which proteins are activated but also the degree to which they are activated over time [50-52]. Data from human exercise trials reveal that AMPK phosphorylation and/or activity increases within ten minutes of starting a continuous bout of exercise, (Figure 1.2B) [53-57] followed by a plateau [56], or an additional increase [53-55, 57], until exercise ends. Following exercise cessation, AMPK phosphorylation progressively declines [55, 56] and returns to baseline within two to three hours [58]. The trend towards increasing AMPK activity during exercise is also evident in in vitro and in vivo murine models [59-62]. Thus, AMPK activity appears dynamic in response to exercise. However, the time course of AMPK activity in response to exercise has yet to be systematically studied. When studying AMPK activity in response to exercise, a model that provides high temporal resolution must be chosen to capture any rapid onset of AMPK activity that may occur. Generally, studies of AMPK in response to exercise feature only a few time points that are insufficient for fully characterizing the AMPK response to exercise. Various model systems such as in vivo, in vitro, and in silico have been developed to investigate the effects of exercise on skeletal muscle cells. In 2008, an in vitro model of exercise using cultured myotubes was developed to investigate the molecular events that occur during exercise with high experimental control [60].

1.5. Experimental systems for studying exercise responses in skeletal muscle

Although all model systems feature advantages, each also has limitations. In vivo models, in which the whole organism of interest is used for experimentation, are typically considered the gold standard because they encompass a whole-body response to exercise. However, as discussed above, only a limited number of muscle biopsies can be ethically sampled from an individual, which limits the time resolution of the data. Therefore, human models do not currently provide sufficient temporal resolution to accurately measure AMPK signaling dynamics in response to exercise [53]. Although in vivo models

developed to study exercise are largely dependent on humans and mice as model systems, other animals including *Drosophila* [63] and *C. elegans* [64] have been used.

In silico modeling, which involves mechanistic computer models, provides insight into what is occurring between experimental data points derived from in vitro or in vivo experimentation [65]. In silico modeling avoids ethical considerations associated with animal and human experimental models, and offers the only way to manipulate variables with absolute control [65]. In silico models, however, require extensive model validation and calibration and are simplified representations of the real system, such that they are unable to mimic the full extent of its complexity. Once established, in silico models provide predictive information that avoids pitfalls of other experimental models at the cost of being a highly simplified representation of a system.

In vitro modeling involves performing techniques outside of the normal biological environment of a living organism. In vitro models allow investigators to control experimental parameters and allow for artificial manipulation of the system using genetic and pharmacological techniques. Additionally, more samples can typically be collected using in vitro models compared to in vivo models. Again, however, limitations do exist. While researchers continually seek ways to improve the physiological relevance of in vitro models [66-69], they nevertheless sacrifice physiological realism at the expense of experimental control and as such, in vitro models may not accurately predict the effect of the entire organism of interest. The decision to choose an in vivo, in vitro, or in silico model must consider the purpose of the experiment considering the advantages and limitations of the different model systems. Ultimately, all scientifically derived concepts must be supported from a body of evidence collected from a spectrum of model systems and approaches.

1.5.1. Electrical pulse stimulation as an in vitro model of exercise

Electrical pulse stimulation (EPS) has recently emerged as a tool for studying exercise in vitro [60, 70-72]. The in vitro exercise model involves passing current through media in contact with cultured skeletal muscle myotubes, which depolarizes the cell membrane and causes contraction. EPS was originally used to study the role of denervation and reinnervation on acetylcholine receptor regulation [73]. Over the past two

decades, EPS has been used with C_2C_{12} myotubes to mimic exercising skeletal muscle [60, 70, 71, 74].

EPS features several benefits for studying the molecular responses to exercise compared to other experimental model systems. With the ability to control the voltage, frequency, pulse duration, and time duration [70, 72], EPS allows for flexible control of stimulation intensity and duration. An in vitro EPS model also provides the ability to collect many samples, such that many stimulation conditions can be studied, and time courses of higher temporal resolution are possible. Therefore, the in vitro EPS model is a promising method to study exercise-mediated responses in skeletal muscle [70, 72].

1.5.2. The C_2C_{12} cell line

C_2C_{12} myotubes are commonly used as a model of adult skeletal muscle. First established in 1977 by Yaffe and Saxel [75], the C_2C_{12} cell line is an immortalized murine myoblast cell line derived from crush-injured thigh muscles of a C3H mouse. C_2C_{12} myoblasts readily proliferate under high serum conditions. Upon serum starvation, C_2C_{12} myoblasts exit the cell cycle and differentiate [76]. Mechanistically, reducing the serum concentration in the cell culture media induces the expression of insulin-like growth factors (IGFs) and inhibits the expression of basic fibroblast growth factor (bFGF) and transforming growth factor (TGF)-β [77]. The changes in growth factors result in the fusion of stellate, mono-nucleated myoblasts into elongated, multi-nucleated contractile myotubes. The C_2C_{12} cell line has been extensively used in experiments involving genetic manipulations [78] and in studies of structural protein dysfunction (e.g., muscular dystrophy) [79]. More recently, researchers have leveraged the ability of C_2C_{12} myotubes to mimic skeletal muscle contraction to develop improved exercise-in-a-dish models [60, 70].

The lack of systematic testing of the duration and conditions under which differentiation of C_2C_{12} cells should be performed prompts concerns about the optimization of the differentiation protocol. Differentiation is usually performed by reducing serum concentrations [60, 62, 70]; however, the differentiation process results in the random alignment of myotubes with a background population of undifferentiated myoblasts. The effect of background myoblasts is not commonly considered but given the potential for them to contribute confounding effects, the degree of differentiation should be maximized.

In addition, control samples featuring pure myoblasts should also be included in experiments to assess the potential for confounding effects. Thus, a need persists to define a standard protocol that results in robust differentiation.

Imaging-based quantitative measurements of differentiation exist. A direct measure is the fusion index, which expresses the number of nuclei incorporated into myotubes as a percentage of total nuclei in the field of view. A less direct measure was proposed by Veliça and Bunce [76], whose method involves staining myotubes dark which increases the number of dark pixels in an image. The increase in dark pixels is quantified and used as a measure of myotube density [76]. The authors recommend that their staining procedure be used as a complement to fusion index because fusion index is a more direct measure of differentiation.

1.5.3. Electrically stimulating C_2C_{12} myotubes elicits exercise-like effects

Electrically stimulating C_2C_{12} myotubes induces visible contraction and elicits several exercise-like effects [70]. Figure 1.3 compares the responses to exercise as elicited by in vitro electrical stimulation and by exercise. Electrical stimulation induces calcium transients as evidenced by increased concentration of calcium in C_2C_{12} myotubes [70, 80]. The increase in calcium and consequent contraction increases the rate of ATP hydrolysis, which in turn leads to increased concentrations of ADP and AMP and activation of AMPK [60-62, 70, 81] . In addition, lactate and glucose oxidation are increased following 24 hours of electrical stimulation [60, 62, 71] as is mitogen-activated protein kinase signaling, glucose uptake, and GLUT4 recycling [60-62, 70, 71]. Importantly, many of the physiological responses to EPS in cultured myotubes are similar to those observed in exercising skeletal muscle in humans [70, 72]. However, some responses observed during in vivo exercise are not reproducible in the C_2C_{12} EPS model. For example, although increased GLUT4 translocation following EPS has been reported [60, 62], concomitant increases in GLUT4 mRNA have not been demonstrated.

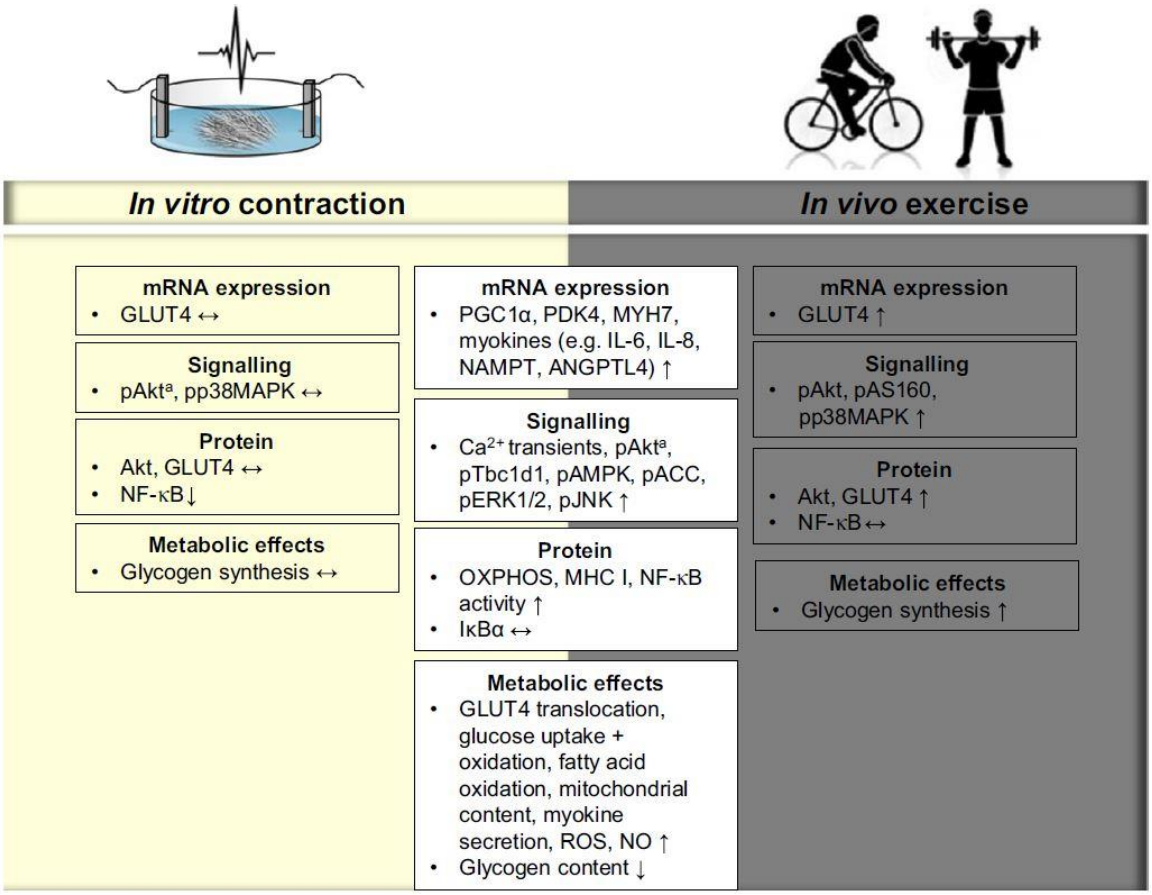

Figure 1.3 Effects of in vitro contraction versus in vivo exercise
Effects that differ between the two model systems appear on the outer columns. Effects common to both model systems appear in the middle. OXPHOS = enzymes of mitochondrial complex. Reprinted with permission [70].

Limitations with this model exist, however. While EPS parameters of 10 Hz, 2-ms pulse duration, and 11.5 V for 1 h elicited a response similar to voluntary wheel running in mice [82], no consensus exists regarding EPS protocols that specifically increase aerobic or anaerobic energy metabolism in C_2C_{12} myotubes [70]. Additionally, the C_2C_{12} cells lack innervation by motor neurons and blood flow. The lack of blood flow (or system perfusion) may enable the local buildup of metabolites that could affect the physiology of the myotubes.

Some of the differences observed between in vitro electrical stimulation and exercise in humans may be resolved by incorporating factors that better recapitulate exercise, such as heat stress and hypoxia. During exercise, the temperature of working muscles can reach 40°C [83] such that mimicking this increase in temperature in the C_2C_{12} cells during electrical stimulation may help lessen the discrepancy between in vivo and in

vitro exercise models. In support of this contention, exposing C_2C_{12} myotubes to one hour of heat stress (40°C) increases AMPK phosphorylation 1.6-fold [83]. The heat exposure additionally increased the expression of PGC-1α and together with the increase in AMPK phosphorylation, may suggest that the heat produced from working muscles may contribute to the adaptive response of skeletal muscle to exercise [83]. Exercise additionally reduces intracellular oxygen due to increased oxygen consumption [84]. Applying cobalt chloride, a hypoxia-mimetic agent, to C_2C_{12} myotubes induces HIF-1α accumulation and AMPK phosphorylation [85], suggesting that the exercise-mediated hypoxic response may be important for skeletal muscle adaptation. Taken together, applying hypoxia and temperature profiles that mimic exercise during electrical stimulation of C_2C_{12} myotubes could address some of the discrepancies between in vitro electrical stimulation and exercise in humans.

Compared to in vivo models, in vitro models of exercise enable small molecules to be applied relatively easily and enable the collection of experimental samples at higher frequencies. Electrical stimulated C_2C_{12} myotubes exhibit many of the responses observed in human muscle in response to exercise. Furthermore, the possibility exists to better mimic in vivo exercise by adding treatments such as hypoxia and enhanced temperature. Altogether, the C_2C_{12} EPS model is a promising tool for simulating exercise responses and studying exercise-mediated signaling dynamics [60, 70-72, 80, 86, 87].

1.5.4. Oxygen levels in cell culture models

Cell culture is typically performed with a partial pressure of oxygen (pO_2) of 141 mmHg (corresponding to an O_2 concentration of 18%, otherwise known as normoxia). However, this pO_2 does not reflect the pO_2 in tissues (physioxia). In vivo, most mammalian tissues experience oxygen levels of 1 to 6% [88]. Skeletal muscle, for example, exhibits a pO_2 of approximately 14 to 25 mmHg (corresponding to an O_2 concentration of 3.4 to 3.8%) [88]. Accordingly, culturing cells at 18% does not accurately represent the in vivo physiological environment [89]. When cells are cultured in normoxia, the pO_2 is up to 10-fold higher than physioxia [88]. The increased pO_2 can increase reactive oxygen species production and decrease oxygen-consuming enzymes such as NAPDH oxidase-4 and nitric oxide synthase [88]. Therefore, the disparity between the pO_2 observed in normoxia and physioxia should be minimized.

A commonly used cellular marker of hypoxia is the expression of hypoxia-inducible factors (HIF). Hypoxia-inducible factors are transcription factors that promote the transcription of target genes associated with erythropoiesis, angiogenesis, glycolysis, and energy metabolism. These genes are expressed during and after exercise [90]. In oxygen-rich environments, hypoxia-inducible factor-1α (HIF1α) is ubiquitinated and targeted for proteasomal degradation, such that HIF1a levels are kept low. In oxygen-poor environments, degradation is inhibited and HIF1α accumulates [90]. Under conditions of accumulation, HIF1α translocates to the nucleus and forms a transcriptionally active complex with HIF1β [90]. HIF1α is easily detected by immunoblotting and therefore provides an easy readout of cellular hypoxia.

Another common technique to measure oxygen concentration in a solution is through the measurement of the dissolved free oxygen [91]. Common methods to detect dissolved oxygen include iodemetric titration [92], the electrochemical method [91], and the optical method [93]. Iodemetric titration involves reacting dissolved oxygen with chemicals that result in the release of iodine. The release of iodine can be measured and used to calculate the dissolved oxygen content [91]. Although iodemetric titration is a classic analytical method, it is cumbersome and cannot provide real-time data [91]. Electrochemical detection uses a defined relationship between an electrode potential and the dissolved oxygen; however, the electrochemical detection is limited because its detection process consumes oxygen [91]. Optical oxygen sensors determine the dissolved oxygen concentration using a fluorescent compound, commonly ruthenium chloride [88, 91]. Light is passed through a fiber optic cable that has the fluorescent compound mounted at the tip (Figure 1.4). The light passing through the fluorescent compound is quenched by dissolved oxygen. The amount of light quenched is proportional to the partial pressure of oxygen [88]. Importantly, oxygen is not consumed during this reaction, therefore a continuous readout of oxygen concentration can be obtained [91, 94].

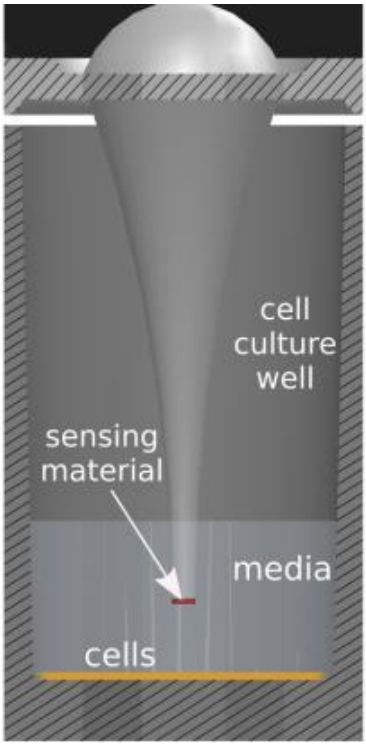

Figure 1.4 Diagram of an optical oxygen sensor within a cell culture well
Light is passed through a fiber optic cable and contacts the sensing material mounted at the probe tip. The light is quenched by the dissolved oxygen in the media and the amount of light quenched is proportional to the partial pressure of oxygen in the media. Reprinted with permission (Lucid Scientific 2019).

Optical oxygen sensing technology provides a suitable approach for determining appropriate incubator atmospheric settings to promote physioxia in the cell culture media. Furthermore, in the C_2C_{12} EPS model, such sensors can be used to indirectly measure the increased cellular respiration expected from contracting myotubes [95]. Decreased pO_2 in the medium in response to electrical stimulation could serve as an indicator that the myotubes are producing energy via oxidative pathways.

1.5.5. Pharmacological tools to study AMPK activity in vitro

A primary advantage of studying AMPK in cultured cells compared to in vivo models is the relative ease in which small molecules can be administered to manipulate AMPK activity. The most commonly used AMPK activator, 5-aminoimidazole-4-carboxyamide-1-b-D-ribofuranoside (AICAR), is readily taken up by cells via the adenosine transporter and phosphorylated by adenosine kinase to generate AICAR 5'-monophosphate (ZMP), an AMP analog [96-99]. Like AMP, ZMP allosterically activates

AMPK by binding to the γ subunit of AMPK. Importantly, ZMP activates AMPK without altering the ADP:ATP or AMP:ATP ratios. ZMP mimics the effect of increased AMP, the levels of which increase during exercise [28], such that AICAR has been used to study exercise-like responses [100]. Although AICAR is commonly used to study AMPK activation, it can also modify other AMP-dependent pathways such as the activity of fructose-1,6-bisphosphatase in the gluconeogenesis pathway [101]. As such, the off-target effects of AICAR must be considered when using this approach to activate AMPK.

To circumvent the non-specific effects of AICAR, a thienopyridone compound, A-769662, was developed. Similar to AMP and AICAR, A-769662 allosterically activates AMPK, however, A-769662 promotes the phosphorylation of Ser-108 within the β1 subunit instead of the Thr-172 of the α subunit [97, 102, 103]. The independent phosphorylation sites of A-769662 and AICAR probably underlie their ability to synergistically activate AMPK when applied together [104]. Unlike AICAR, A-769662 does not compete with adenosine re-uptake into the cell and has an increased specificity for AMPK [102, 103, 105]. Nevertheless, treatment of cells with A-769662 appears to affect their growth and metabolism in an AMPK-independent manner, suggesting that it has some off-target effects [106]. Overall, A-769662 demonstrates the opportunity to develop subunit-specific AMPK activators with increased specificity compared to AICAR and provides an additional method to activate AMPK.

The availability of pharmacological AMPK inhibitors is currently limited. First identified in a high-throughput kinase assay, compound C (also known as dorsomorphin) is the most commonly used AMPK inhibitor [107, 108]. Mechanistically, the binding of compound C to AMPK causes a structural change in the activation loop of the α2 subunit. The conformational change causes partial blockage of the ATP-binding site that is critical for AMPK phosphorylation [108-110]. As such, blocking of the ATP-binding site on the α2 subunit inhibits AMPK activity. Despite the effectiveness of compound C for inhibiting AMPK, it affects numerous other kinases. Compound C has an IC_{50} value of 0.1-0.2 μM, however, the concentration required to completely inhibit AMPK activity is 40 μM [111]. At a concentration of only 2.5 μM, compound C was found to inhibit 54 other kinases by greater than 30% (23 of which >50%) [109]. By virtue of the non-specific effects of compound C, data obtained using this molecule is criticized and some have recommended that its use be avoided altogether [111].

SBI-0206965 was discovered as an AMPK inhibitor with improved potency and kinase selectivity compared to compound C [111]. Like compound C, binding of SBI-0206965 partially blocks the ATP-binding site needed for AMPK activation [109]. Additionally, SBI-0206965 reduces AICAR-mediated AMPK activity, most likely due to decreased uptake of AICAR as evidenced by reduced intracellular ZMP concentration [109]. In a recent report, compound C and SBI-0206965 were profiled against 50 kinases. The two molecules exerted the highest inhibitory effects on AMPK [109]. However, SBI-0206965 inhibited only five other kinases by >50% compared to 23 by compound C [109]. The use of SBI-0206965 together with AICAR is not recommended. However, the authors justified their recommendation based on the SBI-0206965-mediated impairment of AICAR transport into cells [111]. The possibility exists that this issue could be circumvented by adding AICAR prior to SBI-0206965.

Overall, compounds such as AICAR and compound C have profound effects on AMPK activity that can be leveraged to study the effects of AMPK activity on downstream targets. However, pharmacological approaches to studying AMPK activity are limited by specificity and potency, which may affect the validity of the data that arises from their use. The use of small molecules must therefore be judiciously validated for the intended application.

1.6. Aims and hypotheses

The overarching goal of this thesis was to develop an in vitro model of exercise that can be used to study the dynamics of AMPK signaling in response to exercise. The specific aims were to:

- Validate EPS of C_2C_{12} myotubes as a method for inducing AMPK signaling.
- Determine the extent to which AMPK signaling can be manipulated using small-molecule activators and inhibitors.
- Characterize the time course of AMPK signaling during and post- EPS in cultured myotubes.

Each aim is associated with the following corresponding research hypotheses:

- That EPS increases ATP turnover, which elicits exercise-like AMPK signaling in C_2C_{12} myotubes.

- That small-molecule activators and inhibitors increase and decrease AMPK signaling, respectively.

- That AMPK signaling in electrically stimulated C_2C_{12} increases during the initial minutes of electrical stimulation, followed by achieving steady state, and then decreases dynamically during recovery back to resting levels.

Chapter 2. Materials and methods

2.1. Materials

All chemicals were purchased from Sigma, VWR, and Fischer Scientific. Unless otherwise stated, the antibodies, AICAR (9944P), and lambda protein phosphatase (50811856) were from Cell Signaling Technologies (New England BioLabs). Cell culture plastics were from VWR. Compound C was from Sigma. A-769662 (11900) and SBI-0206965 (18477) were from Cayman Chemical Co.

2.2. Cell culture

C_2C_{12} myoblasts (ATCC # CRL-1772, lot 70004012, passage no. 8-12) were thawed in a 37ºC water bath and transferred to a 10-cm cell culture dish containing growth media. Growth media consisted of Dulbecco's modified Eagle's medium (DMEM; Corning: 50-003-PC) supplemented with 10% fetal bovine serum (VWR: 97068-085). Cells were maintained at 37ºC in a 5% CO_2, ~16% O_2, and 80% humidified atmosphere unless otherwise stated. For differentiation, cells were seeded in 35-mm dishes at a density of 100,000 cells/mL, for a total of 300,000 cells per well. The myoblasts were maintained in growth media until reaching ~90% confluency, at which point the media was replaced with differentiation media. Differentiation media consisted of DMEM supplemented with 2% horse serum (ATCC: 30-2040). Differentiation media was replaced every other day for a total of five days of differentiation.

2.3. Jenner–Giemsa staining

Cell culture was performed as described above. Jenner-Giemsa staining was performed as described previously [76]. Both the Jenner and Giemsa dyes contain methylene blue and eosin [76]. Methylene blue binds to negatively charged particles such as DNA [112] which stains nuclei light pink. Eosin binds to eosinophilic compounds such as amino acid residues that contain arginine and lysine [113] which result in darkly stained myotubes [76]. To perform this stain, cells were rinsed twice with phosphate buffered saline (PBS), fixed in 100% methanol for five minutes, and left to air-dry. Jenner stain (Electron Microscopy Sciences: 26114-01) was diluted 1:3 in PBS (pH 5.6) and Giemsa

stain (Electron Microscopy Sciences: 26114-02) was diluted 1:20 in PBS (pH 5.6). One millilitre of the Jenner stain was incubated in the wells for five minutes at 37^{o}C followed by washing with distilled water. Next, 1 mL of Giemsa stain was incubated in the wells for 10 min at room temperature before washing again with distilled water.

2.3.1. Myotube density

Jenner-Giemsa solutions stain myotubes dark, and as such will increase the number of dark pixels. As such, using the histogram feature of ImageJ, the number of pixels below an intensity of 75 were calculated as a measure of myotube density [76, 114]. The final myotube density for each well was an average of four random images per well captured using an inverted microscope (Etaluma: LS560; San Diego, CA).

2.4. Electrical stimulation

C_2C_{12} myotubes differentiated for five days were placed in a hypoxia workstation (Baker Ruskinn; Sanford, ME) and equilibrated to 16% O_2, 5% CO_2, 80% humidity, and 37^{o}C for at least one hour. Equilibration was confirmed using optical oxygen sensors immersed in the culture media (Lucid Scientific; Atlanta, GA; described below). Electrical stimulation was applied using the C-Pace EP system (IonOptix; Milton, MA) with C-dishes for 35-mm dishes and the stimulation parameters set to 20 V, 2 ms, and 1 Hz [60, 71]. An inverted digital microscope was used to monitor contraction (Etaluma; San Diego, CA). At the end of electrical stimulation experiments, the cells were rinsed twice with ice-cold PBS, immersed in liquid nitrogen and immediately transferred to a -80^{o}C freezer for storage.

2.5. Oxygen sensing

Oxygen levels in cell culture media were monitored using optical oxygen sensors (Lucid Scientific; Atlanta, GA). The oxygen sensors were calibrated according to the manufacturer instructions. In brief, a 0.8 mM solution of Na_2SO_3 in PBS was prepared. Na_2SO_3 binds to oxygen creating a zero-oxygen environment. With stirring, the Na_2SO_3 solution saturates with oxygen, such that the solution pO_2 rises to ambient oxygen levels in approximately 16 hours. The zero and ambient oxygen readings are then used to calibrate the sensors.

To obtain accurate measurements, the sensors must be situated as close to the cell layer as possible (W. Inman, Lucid Scientific, personal communication). The sensors were positioned by mounting them through the lid of a 35-mm cell culture dish and a small piece of rubber glued to the dish lid. This set up facilitated the vertical adjustment of sensor so that it could be set at a pre-determined distance from the bottom of the cell culture dish. A piece of glass 640 or 320 microns thick was placed in an empty cell culture dish. The sensor was pushed down through the lid and rubber until it touched the glass. The sensor (with the lid) was then transferred to the 35-mm dish containing the sample to be measured, with the sensor positioned at the pre-determined distance from the bottom of the dish.

2.6. Immunoblot analysis

AMPK signaling was operationally defined as the increased levels of phosphorylated AMPK, ACC, and TBC1D1. ACC is phosphorylated by various kinases, however, AMPK phosphorylates ACC on an AMPK-specific site (Ser-79) [115]. In contrast, TBC1D1 phospho-sites are not unique to AMPK, but TBC1D1 Ser-231 and Ser-700 represent consensus matches for the AMPK phosphorylation motif [116]. Furthermore, it has been suggested that TBC1D1 regulation to occur primarily by AMPK [116]. Therefore, ACC and TBC1D1 phosphorylation on Ser-79 and Ser-231 (equivalent to the Ser-237 in human TBC1D1), respectively, are likely phosphorylated primarily by AMPK under my experimental conditions.

The expression and phosphorylation of proteins were analyzed by immunoblotting. Cells were removed from -80^{o}C storage and thawed on ice for two minutes. To each 35-mm dish,150 µL of NP-40 lysis buffer was added (50 mM Tris, 400 mM NaCl, 1 mM EDTA, 1% NP-40 alternative, 15% glycerol, 50 mM β-glycerophosphate, 10 mM NaPP, 30 mM NaF, 100 µM Na_3VO_4, 1X Roche cOmplete Protease inhibitor cocktail (Cat. # 11836170001), and 1X Sigma phosphatase inhibitor cocktail 3 (Cat. # P0044)). Cells were scraped and transferred to a pre-chilled microfuge tube. The samples were agitated at 4^{o}C for 30 minutes. The supernatant was collected and frozen at -80^{o}C until analysis. Protein concentration was determined using a bicinchoninic acid assay (Pierce). Cell lysates were loaded into an 8-10% sodium dodecyl sulfate–polyacrylamide gel and subjected to electrophoresis (Bio-Rad: 1658004EDU and 1656001; 1-2 hours at 150 V). Proteins were transferred to a low fluorescent-polyvinylidene difluoride membrane (GE Healthcare

Biosciences: 10600022) via wet transfer (Bio-Rad: 1658004EDU and 1704071; 100 V for 1-1.5 hours). 2,2,2-Trichloroethanol was added to the SDS-PAGE gel to visualize proteins after ultraviolet light exposure (the “stain-free” method) [117]. The membrane was blocked with 5% non-fat dry milk (Cell Signaling: 9999) in Tris-buffered saline containing 0.1% Tween-20 (TBS-T). The blots were incubated overnight at 4^{o}C with the primary antibody [anti-AMPK (2532S, 1:500, lot 19), anti-phospho-AMPK (2535S, Thr-172, 1:300, lot 21), anti-ACC (3676S, 1:500, lot 9), anti-phospho-ACC (11818S, Ser-79, 1:300, lot 4), anti-TBC1D1 (66433S, 1:500, lot 1), anti-phospho-TBC1D1 (Sigma; 07-2268, Ser-237 1:200, lot 3120117)]. The blots were washed three times for five minutes each with TBS-T and then incubated with anti-mouse IgG (1:3000) conjugated to horseradish peroxidase. The blots were again washed three times for five minutes each with TBS-T and incubated with ECL substrate (Bio-Rad: 1705061) for five minutes. The blots were visualized using a chemiluminescence detector (Licor: 3600-00 and Bio-Rad: 12003154).

2.6.1. Quantification of immunoblots

Quantification of western blots was performed using ImageJ [114]. First, the total protein of each lane from the stain-free blot was determined using the integrated density measurement tool in ImageJ [117, 118]. Second, a normalization factor was determined by dividing the minimum value of all lanes of interest by each lane. The phospho- and total protein blots were then quantified using the gel analysis tool in ImageJ. The intensity of each band was then normalized using the normalization factor. The resulting band intensity reflected the intensity of the band normalized to the total protein of the lane (Figure 2.1). For phospho-protein normalization to total protein, the level of phospho-protein was divided by the level of total protein.

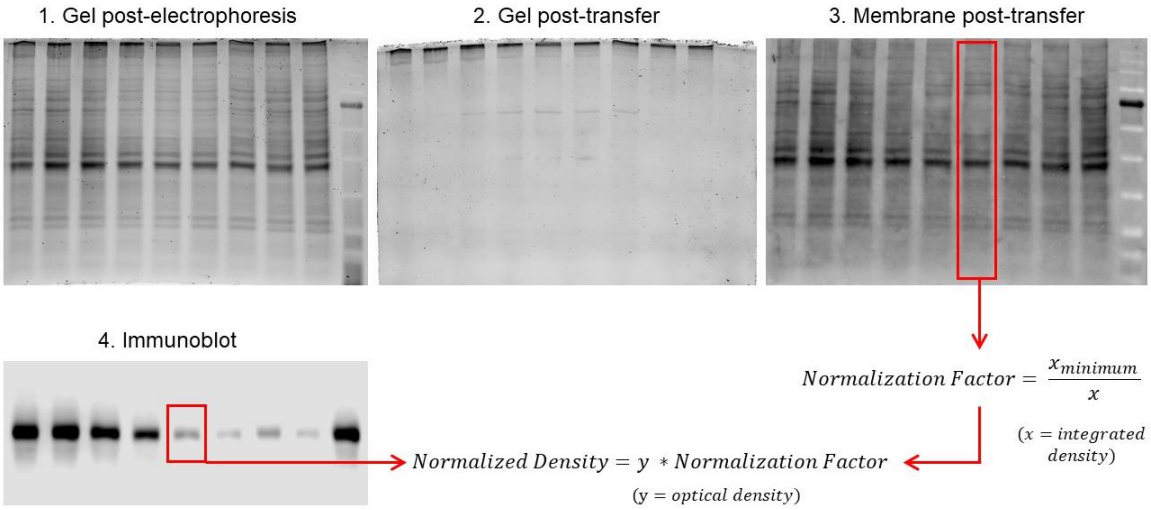

Figure 2.1 Workflow to quantify immunoblots using stain-free technology
Immunoblotting is performed as described in the methods section. In brief, proteins are separated via gel electrophoresis and visualized by exposing the gel to ultraviolet light for two minutes. Proteins are transferred to a low-fluorescent PVDF membrane. A normalization factor is calculated using the integrated density of each lane of the membrane. Finally, the optical density of the band of interest is normalized using the respective normalization factor.

2.7. Cell metabolite and toxicity assays

Release of L-lactate into previously frozen cultured media of stimulated myotubes was measured using a glycolysis cell-based assay kit (Cayman Chemical Co.: 600450). Absolute values of L-lactate concentrations were determined using serial dilutions of a known L-lactate concentration. The intracellular ATP concentration of frozen C_2C_{12} myotubes was measured using a cellular ATP measurement kit (Cayman Chemical Co.: 700410). Absolute values of ATP concentrations were determined using serial dilutions of a known ATP concentration. Cytotoxicity was analyzed by measuring levels of lactate dehydrogenase (LDH) into previously frozen cultured media of stimulated myotubes. LDH measurements were performed with the Cytotoxicity Detection Kit Plus (Roche: 4744926001). L-lactate, LDH, and ATP assay protocols are documented in the Appendix.

2.8. Statistical analysis

Statistical comparisons between treatment groups were performed using R version 3.6.1 [119]. A linear mixed effects model was constructed with time as a fixed effect and batch as a random effect using the *lmer* function from the *lme4* package [120]. The batch term represented experimental replicates that were performed on different days with

different freeze-thaw batches of cells and different batches of cell culture media. Assumptions of normality, independence, and homoscedasticity were verified prior to analysis. Tests of hypothesis include an omnibus F-test on the model followed by post-hoc comparisons between treatment groups, which were analyzed with unpaired t-tests corrected for multiple comparisons using the Tukey method. Statistical significance was set at $p<0.05$. Data are presented as either the raw data or the mean ± 95% confidence interval as indicated in the corresponding figure caption. The R code for all figures and statistical analyses, and the raw data are documented in the Appendix.

Chapter 3. Results

3.1. C_2C_{12} myoblasts differentiated into contractile myotubes in response to the differentiation protocol

Two analyses were performed to determine the extent to which the C_2C_{12} myoblasts differentiated into contractile myotubes in response to the differentiation protocol. First, Jenner-Giemsa staining was used to quantify myotube density. Second, the contractile response of the myotubes to electrical stimulation (20 V, 2 ms, 1 Hz) was assessed by live-cell imaging. Myoblasts and myotubes were differentiated for five days, with samples collected on each day and stained and imaged (Figure 3.1: A - H). Histograms of myotube density (Figure 3.2) revealed a peak at day four of differentiation (Figure 3.3). Myotubes differentiated for five days (Video 1) were contractile in response to electrical stimulation (Video 2).

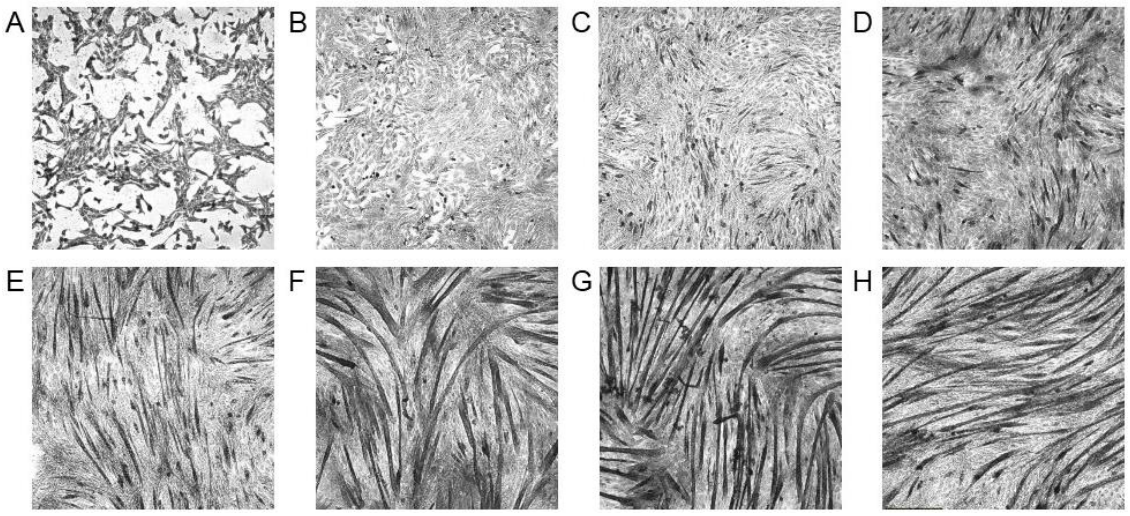

Figure 3.1 Images of differentiating C_2C_{12} myoblasts into myotubes
C_2C_{12} cells were stained with Jenner-Giemsa stain on each day of a five-day differentiation protocol. A – H: differentiation of C_2C_{12} myoblasts into myotubes from day -2 to day 5, respectively. Growth media was replaced with differentiation media on day 0. Data are from a single experiment.

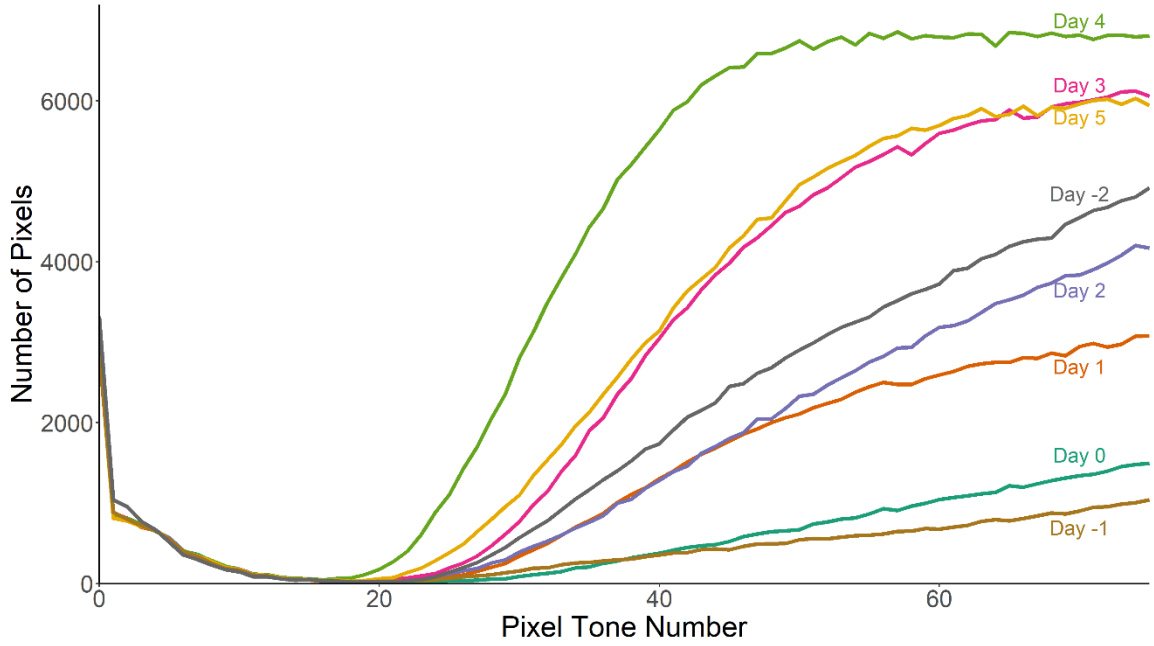

Figure 3.2 Histogram of pixels ≤ 75 from Jenner-Giemsa stained C_2C_{12} cells differentiating over five days

Quantification of images A – H in Figure 3.1. Jenner-Giemsa stains myotubes dark (pixels ≤ 75). A leftward shift in the histogram means more dark pixels. Data are from a single experiment. A. U. = arbitrary units.

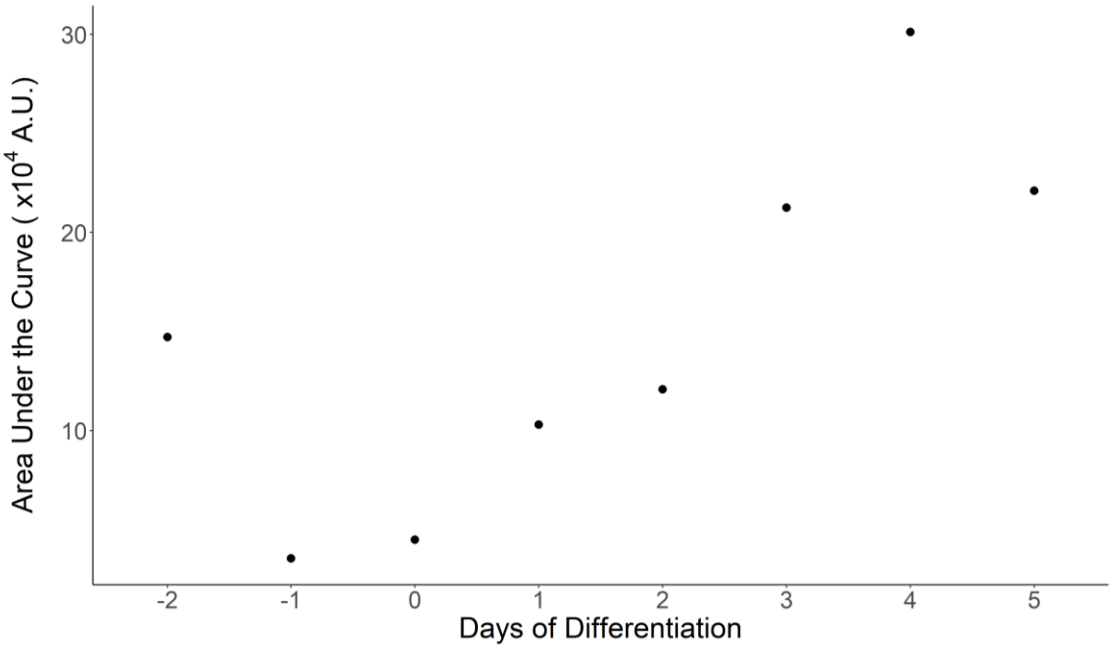

Figure 3.3 Histogram analysis of differentiating C_2C_{12} cells over five days

Pixels ≤ 75 from day -2 to day 5 of differentiating C_2C_{12} cells (area under the curves from Figure 3.2). Growth media was replaced with differentiation media on day 0. Data are from a single experiment. A. U. = arbitrary units.

Video 1 **Differentiation of C_2C_{12} myoblasts into myotubes**

C_2C_{12} were seeded in a 35-mm dish and allowed to proliferate until ~80% confluency. Growth media was then replaced with differentiation media and the myoblasts fused into contractile myotubes. 10X magnification. To open the video, hold *CTL* and click on the thumbnail.

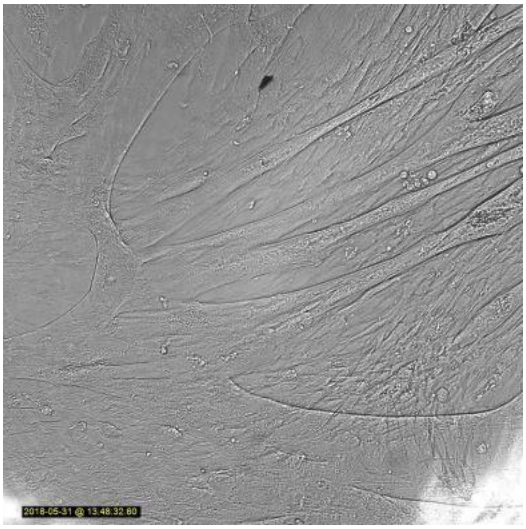

Video 2 **Contraction of C_2C_{12} myotubes**

C_2C_{12} myotubes differentiated for five days were electrically stimulated (20 V, 2 ms, 1 Hz) and imaged using an inverted digital microscope. 10X magnification. To open the video, hold *CTL* and click on the thumbnail.

3.2. Antibody validation

To determine the appropriate amount of protein to load for western blotting, I performed serial dilutions of a pooled cell lysate from stimulated C_2C_{12} myotubes. The span of signal intensities that display a linear relationship between the mass of protein loaded and the intensity of the signal for all phospho-antibodies was 18 to 25 µg (shaded

area in Figure 3.4). I then verified the phospho-specificity of the phospho-antibodies by incubating western blots probed with the phospho- and total protein with lambda protein phosphatase. Lambda protein phosphatase cleaves phosphate groups from serine, threonine, and tyrosine residues. As such, if the antibodies are phospho-specific, no signal should be detected after treatment with lambda protein phosphatase. Treatment with lambda protein phosphatase caused no difference in the signal for total AMPK, ACC, and TBC1D1, but eliminated all signal for p-AMPK and p-TBC1D1 and reduced the signal for p-ACC (Figure 3.5).

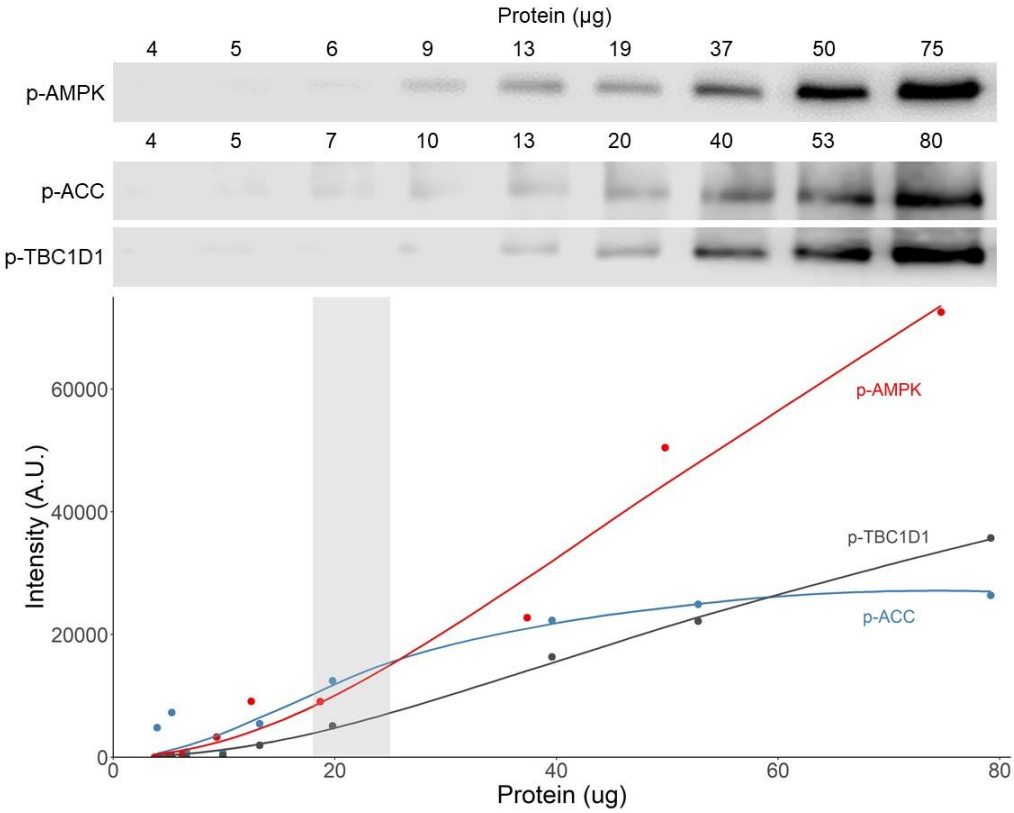

Figure 3.4 Linear dynamic range of p-AMPK, p-ACC, and p-TBC1D1 antibodies
A pooled cell lysate of electrically stimulated C_2C_{12} myotubes was serially diluted and subjected to immunoblotting. Shaded area (18 to 25 µg) represents combined linear range of detection for all three antibodies. Representative blot of p-AMPK above. Data are from a single experiment. A. U. = arbitrary units.

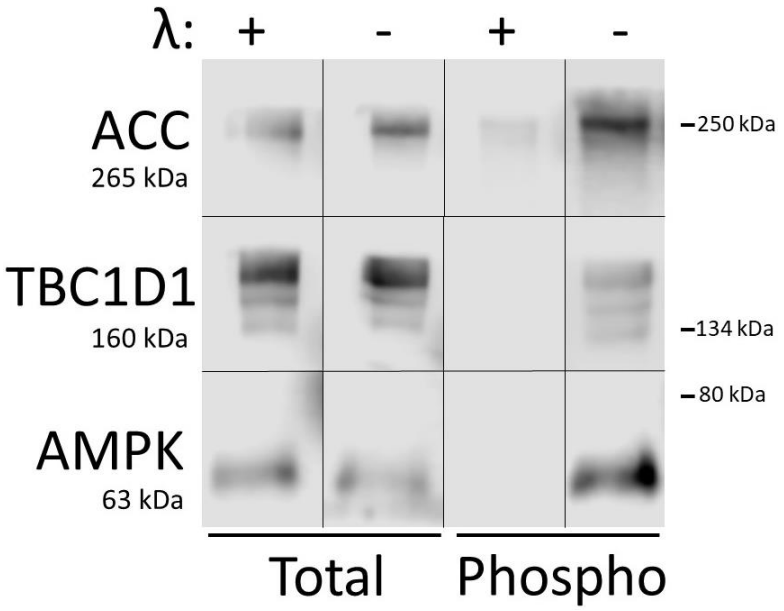

Figure 3.5 Phospho-specificity of p-AMPK, p-ACC, and p-TBC1D1 antibodies
Immunoblot membranes were incubated with (-) and without (+) lambda protein phosphatase (λ) followed by detection. Data are from a single experiment.

3.3. AMPK signaling is observable in C_2C_{12} myotubes

To test whether AMPK could be activated in C_2C_{12} myotubes, I treated the cells with increasing doses of two small-molecule AMPK activators, AICAR and A-769662. AICAR maximally activated p-AMPK, p-ACC, and p-TBC1D1 at 1.25, 10, and 10 mM, respectively (Figure 3.6 and Figure 3.7). I fit a Hill equation to the p-ACC data from the AICAR treatment, which resulted in a 90% effective concentration (EC_{90}) estimate of 2.6 mM (Figure 3.7). A-769662 maximally activated p-AMPK, p-ACC, and p-TBC1D1 at 666 µM (Figure 3.8). Figure 3.9 illustrates changes in AMPK signaling resulting from treatment with AICAR, A-769992, EPS, and all three together. Compared to vehicle treatment, AMPK signaling increased with 125 µM A-769662. Compared to 125 µM A-769662, AMPK signaling increased with 2.5 mM AICAR. A 30-second bout of air exposure (cell starvation) increased AMPK phosphorylation (Figure 3.10). Moreover, five seconds or less of air exposure (the typical duration for which the myotubes were exposed to air prior to freezing) did not increase AMPK phosphorylation. EPS did not increase AMPK signaling compared to vehicle. Addition of 2 mM AICAR or 100 µM A-769662 to stimulated myotubes increased AMPK signaling compared to stimulation alone. Addition of 2 mM AICAR and 100 µM A-769662 to stimulated myotubes increased AMPK signaling greater than stimulated myotubes with the compounds alone.

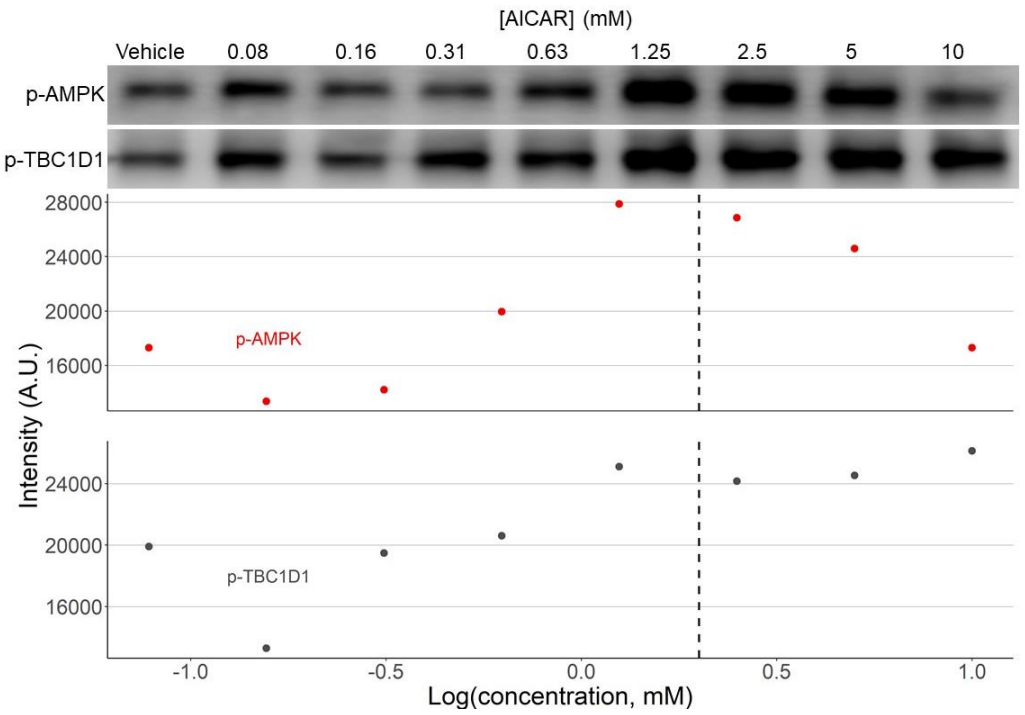

Figure 3.6 Phosphorylation of AMPK and TBC1D1 in response to AICAR
C_2C_{12} myotubes differentiated for five days were incubated with serially diluted AICAR. Cell lysates were subjected to immunoblotting and the levels of p-AMPK and p-TBC1D1 were quantified by densitometry. The dashed line represents the concentration of AICAR commonly used to activate AMPK (2 mM). The p-AMPK and p-TBC1D1 immunoblots are shown above. Data are from a single experiment. A. U. = arbitrary units.

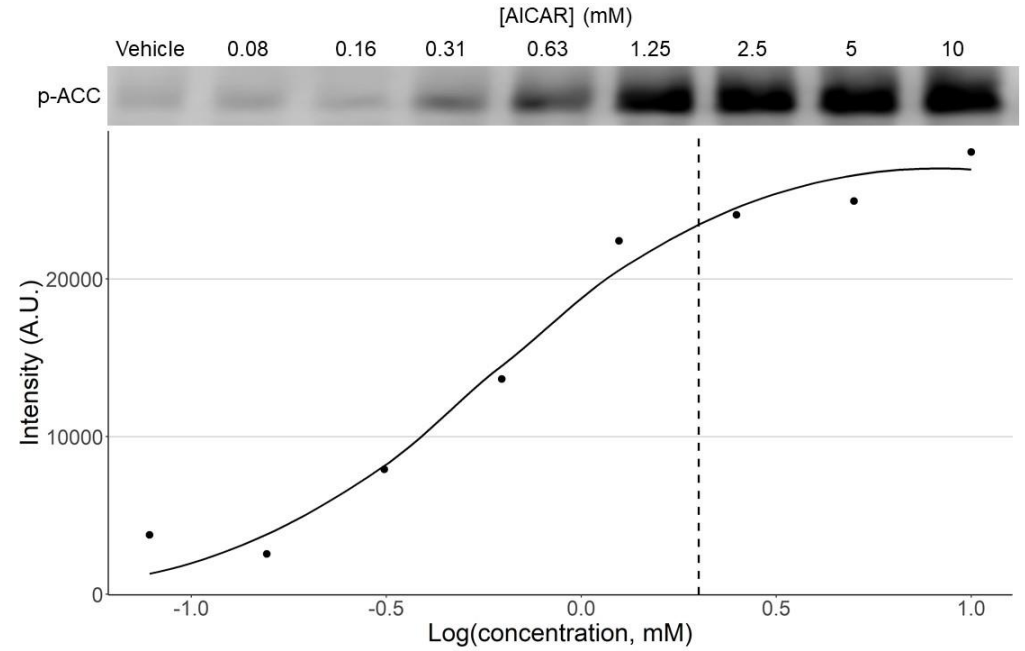

Figure 3.7 Dose-response relationship for p-ACC with AICAR treatment
C_2C_{12} myotubes differentiated for five days were incubated with of the indicated doses of AICAR. Cell lysates were subjected to immunoblotting and the levels of p-ACC were quantified by

densitometry. The experimental data points are overlaid with a black line representing a model fit using the Hill equation. The model parameters were as follows: Ymax = 2.75 x 10^4, n = 1.46, K = 0.577. The dashed line represents the concentration of AICAR commonly used to activate AMPK (2 mM). The p-ACC immunoblot is shown above. Data are from a single experiment. A. U. = arbitrary units.

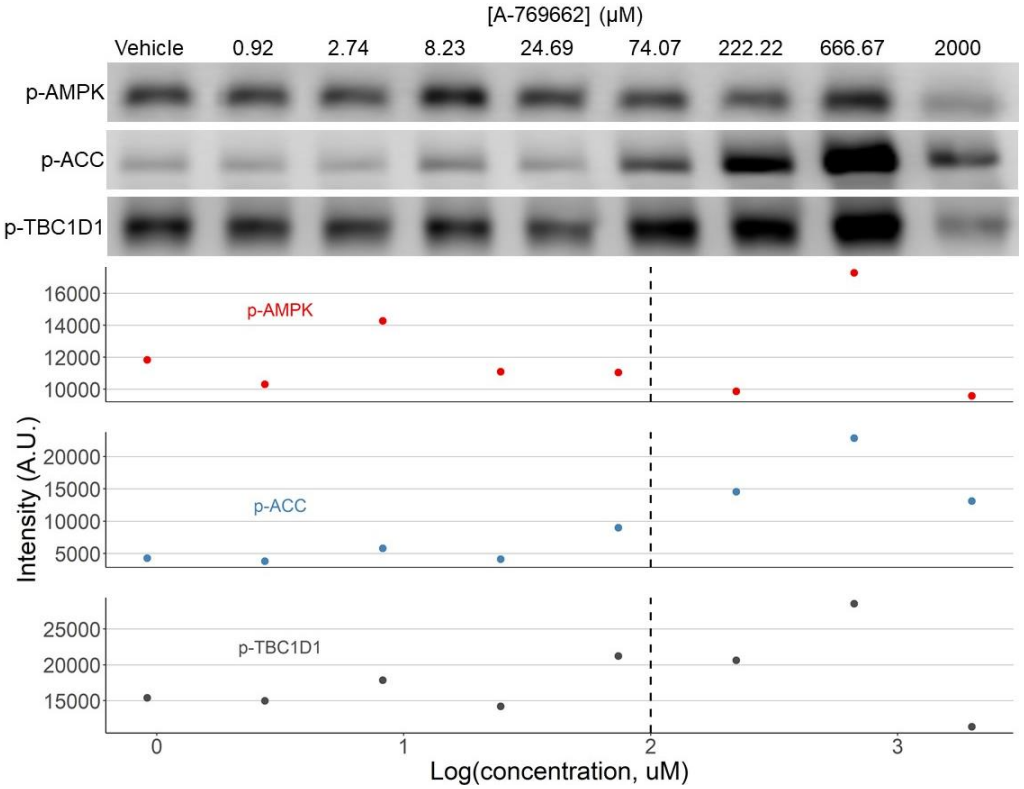

Figure 3.8 AMPK signaling in response to A-769662

C_2C_{12} myotubes differentiated for five days were incubated with the indicated doses of A-769662. Cell lysates were subjected to immunoblotting and levels of p-AMPK, p-ACC, and p-TBC1D1 were quantified by densitometry. The dashed line represents the concentration of A-769662 commonly used to activate AMPK (100 μM). The p-AMPK, p-ACC, and p-TBC1D1 immunoblots are shown above. Data are from a single experiment. A. U. = arbitrary units.

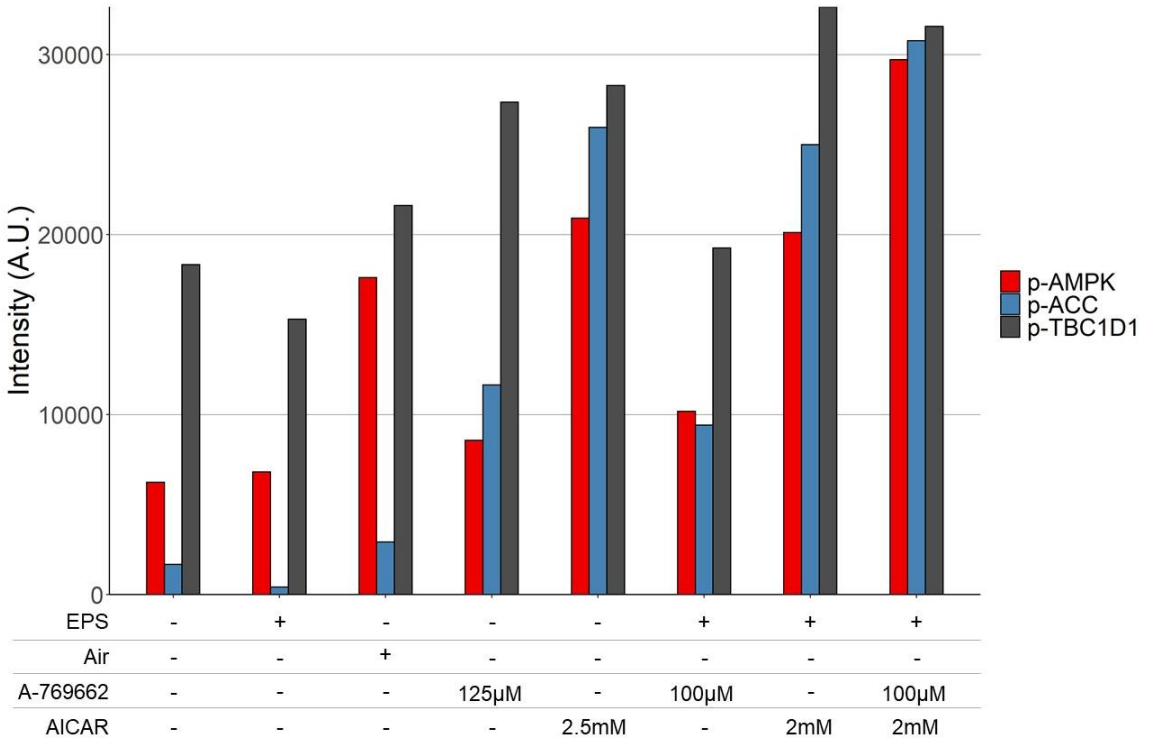

Figure 3.9 AMPK signaling in response to various activating treatments

C_2C_{12} myotubes differentiated for five days were applied various treatments to activate AMPK. Cell lysates were subjected to immunoblotting and levels of p-AMPK, p-ACC, and p-TBC1D1 were quantified by densitometry. Air = 30 seconds of air exposure. EPS = electrical pulse stimulation (20 V, 2 ms, 1 Hz, 60 min). Data are from a single experiment. A. U. = arbitrary units.

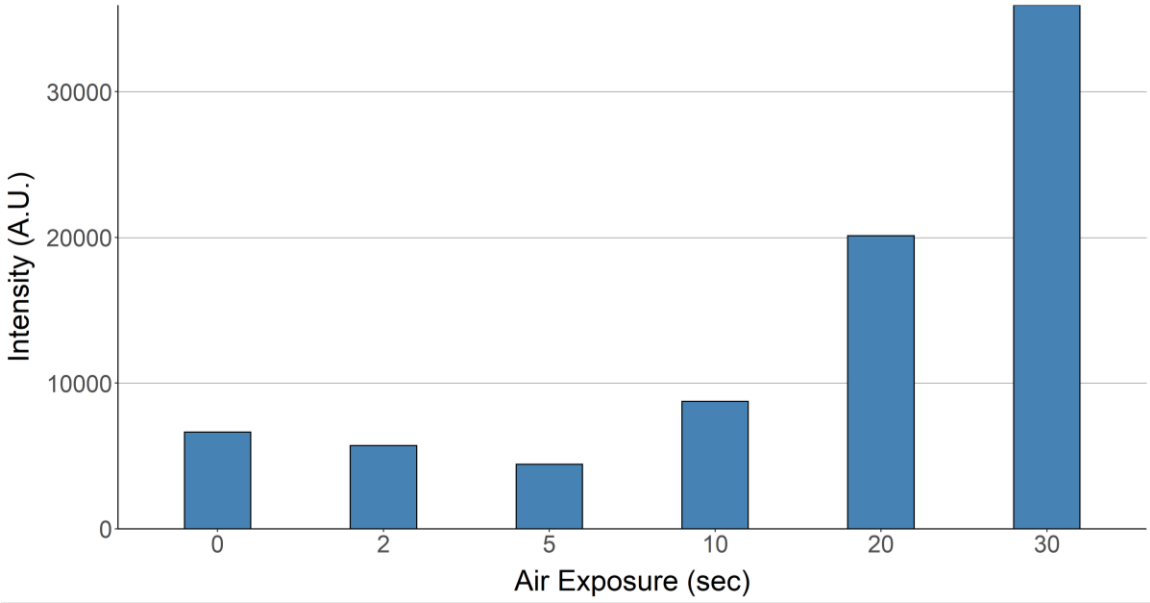

Figure 3.10 AMPK phosphorylation following air exposure

C_2C_{12} myotubes differentiated for five days were exposed to air by removing the cell culture media. Cell lysates were subjected to immunoblotting and the levels of p-AMPK were quantified by densitometry. Data are from a single experiment. A. U. = arbitrary units.

3.4. AMPK signaling can be inhibited in C_2C_{12} myotubes

To test whether AMPK signaling could be inhibited in C_2C_{12} myotubes, I applied different doses of compound C and SBI-0206965 to C_2C_{12} myotubes pre-activated with 2 mM AICAR for 30 minutes. I observed that compound C maximally inhibited p-AMPK, p-ACC, and p-TBC1D1 at 62.5, 1,000, and 31.25 µM, respectively (Figure 3.11). SBI-0206965 maximally inhibited p-ACC and p-TBC1D1 at 111.11 and 333.33 µM, respectively (Figure 3.12 and Figure 3.13). AMPK phosphorylation increased with increasing concentrations of SBI-0206965 (Figure 3.12). A Hill equation fit to the p-ACC data from SBI-0206965 resulted in an IC_{10} estimate of 49.25 µM (Figure 3.13).

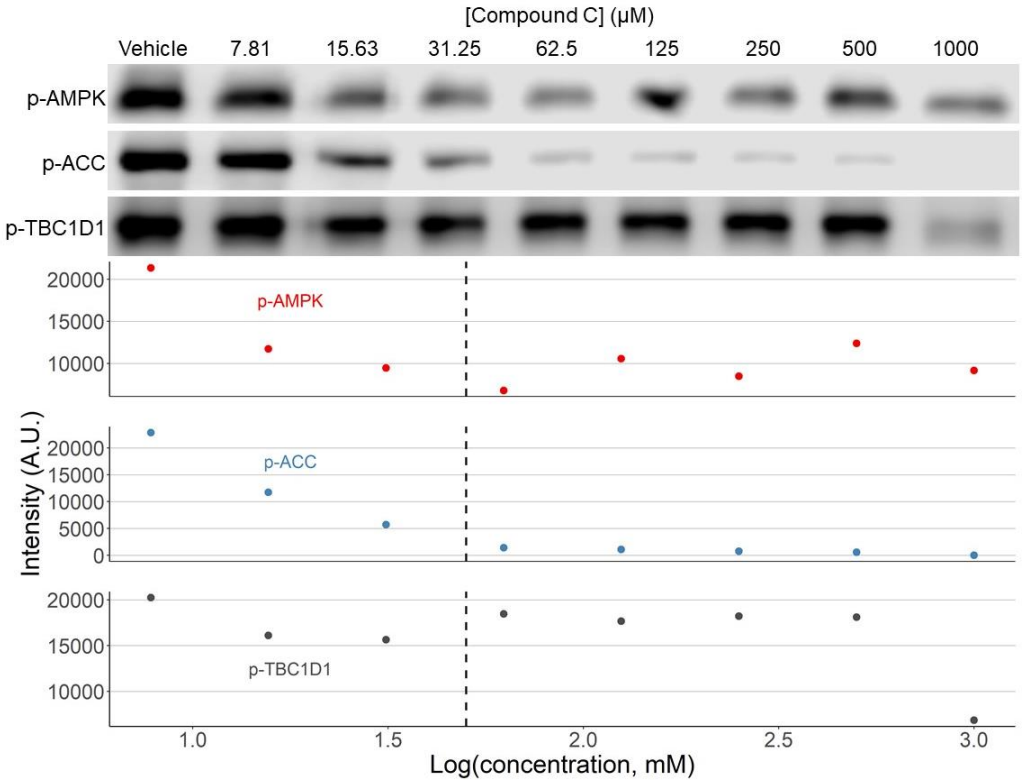

Figure 3.11 AMPK signaling in response to compound C

C_2C_{12} myotubes differentiated for five days were pre-treated with AICAR (2 mM) for 30 minutes after which serially diluted amounts of compound C were applied for 30 minutes. Cell lysates were subjected to immunoblotting and levels of p-AMPK, p-ACC, and p-TBC1D1 were quantified by densitometry. The dashed line represents the concentration of compound C commonly used to inhibit AMPK (50 µM). The p-AMPK, p-ACC, and p-TBC1D1 immunoblots are shown above. Data are from a single experiment. A. U. = arbitrary units.

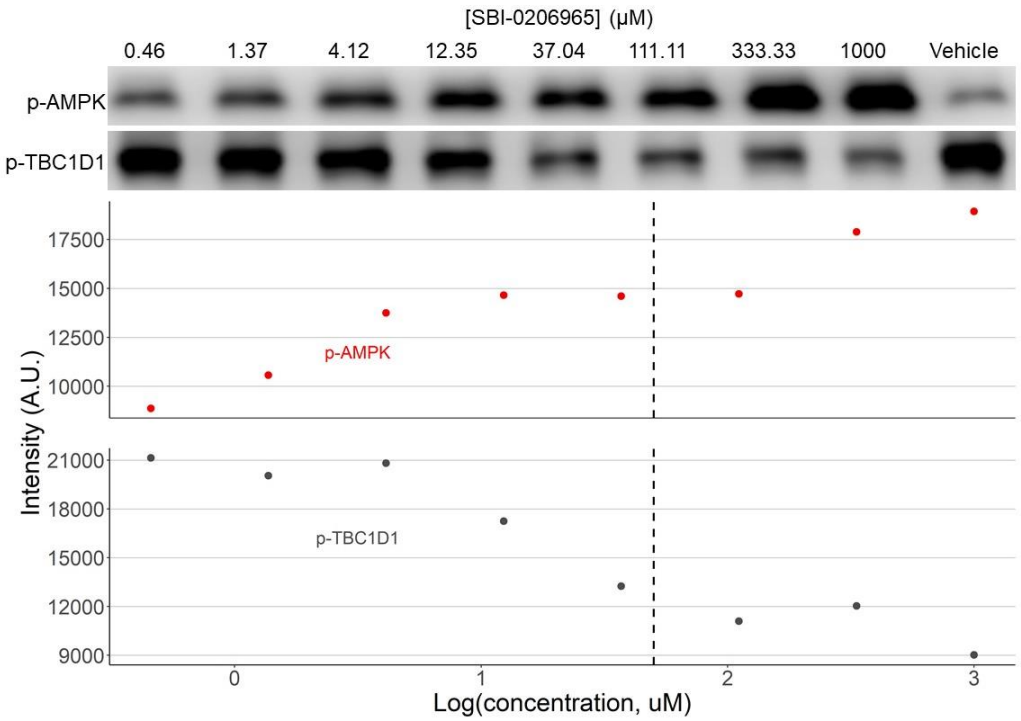

Figure 3.12 Phosphorylation of AMPK and TBC1D1 in response to SBI-0206965
C_2C_{12} myotubes differentiated for five days were pre-treated with AICAR (2 mM) for 30 minutes after which serially diluted amounts of SBI-0206965 were applied for 30 minutes. Cell lysates were subjected to immunoblotting and levels of p-AMPK and p-TBC1D1 were quantified by densitometry. The dashed line represents the concentration of SBI-0206965 commonly used to inhibit AMPK (50 μM). The p-AMPK and p-TBC1D1 immunoblots are shown above. Data are from a single experiment. A. U. = arbitrary units.

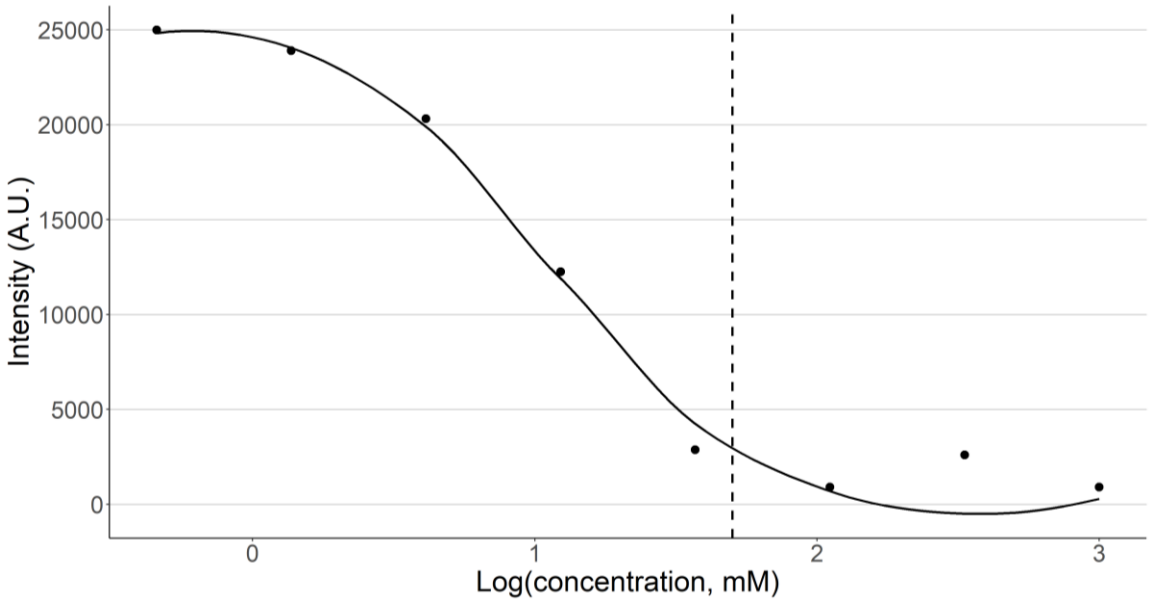

Figure 3.13 Dose-response relationship for p-ACC with SBI-0206965 treatment
C_2C_{12} myotubes differentiated for five days were pre-treated with AICAR (2 mM) for 30 minutes after which the indicated doses of SBI-0206965 were applied for 30 minutes. Cell lysates were

subjected to immunoblotting and levels of p-ACC were quantified by densitometry. Experimental data points overlaid with a model fit to the Hill equation. The model parameters were as follows: Ymax = 2.50 x 10^4, n = 1.51, K = 39.2. The dashed line represents the concentration of SBI-0206965 commonly used to activate AMPK (50 µM). The p-ACC immunoblot is shown above. Data are from a single experiment. A. U. = arbitrary units.

3.5. EPS causes C_2C_{12} myotubes to consume oxygen

To investigate whether EPS stimulates energy-producing metabolic pathways in C_2C_{12} cells, I measured the pO2 in the cell culture media. Additionally, I collected media and cell lysates before and after electrical stimulation (20 V, 2 ms, 1 Hz, 180 min), and after three hours of recovery (Figure 3.18) for L-Lactate (a measure of glycolytic flux) and intracellular ATP measurements. To assess oxygen consumption, I measured the pO_2 in the culture media overlaying C_2C_{12} myotubes in response to electrical stimulation (90 minutes at 20 V, 1 Hz, and 2 ms) at two different atmospheric O_2 concentrations (16% and 8%). At 16% oxygen, the pO_2 in the media of contracting C_2C_{12} myotubes was reduced compared to non-stimulated myotubes (Figure 3.14, compare yellow and black lines). The decrease in pO_2 of contracting myotubes was also observed in the 8% atmospheric pO_2 condition. Similar trends were observed when the experiment was repeated in reverse (Figure 3.15), with the exception that the contracting myotubes at 16% exhibited higher overall pO_2 compared to the resting myotubes. Intracellular ATP measurements revealed no statistical difference at any of the time points ($p = 0.389$, Figure 3.16). Lastly, the concentrations of secreted L-Lactate were not statistically different at any of the time points ($p = 0.903$, Figure 3.17).

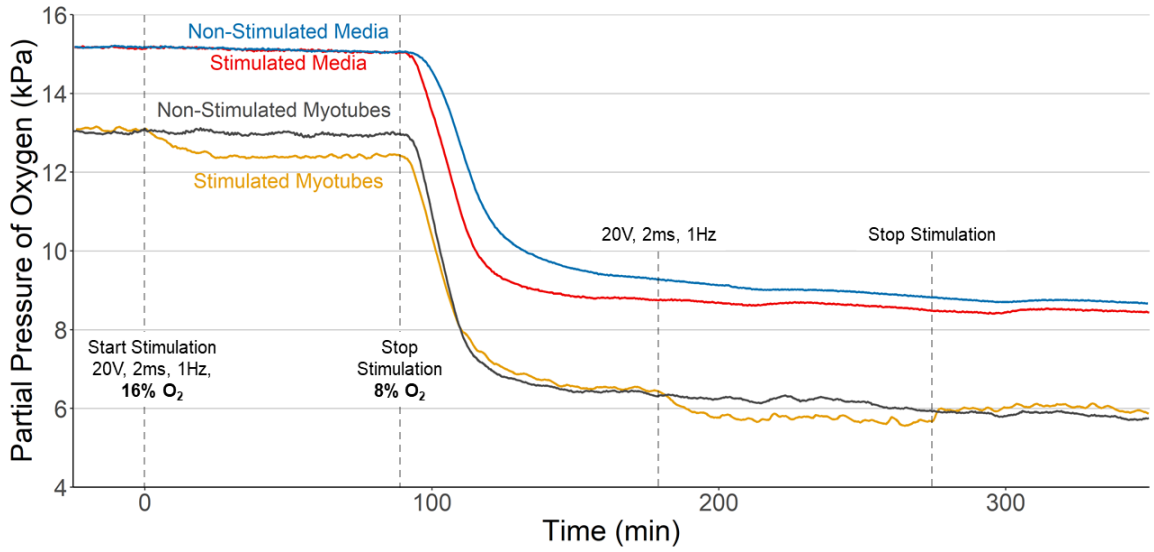

Figure 3.14 Oxygen partial pressure kinetics of contracting C_2C_{12} myotubes in 16% and 8% O_2 atmospheres

Partial pressures of oxygen were measured in the culture media of dishes with and without cultured C_2C_{12} myotubes and with and without EPS (20 V, 2 ms, 1 Hz). The atmospheric oxygen was set to 16% and EPS was applied for 90 minutes. The stimulation was stopped and the atmospheric O_2 was changed to 8%. After 90 minutes of equilibration, EPS was applied for another 90 minutes.

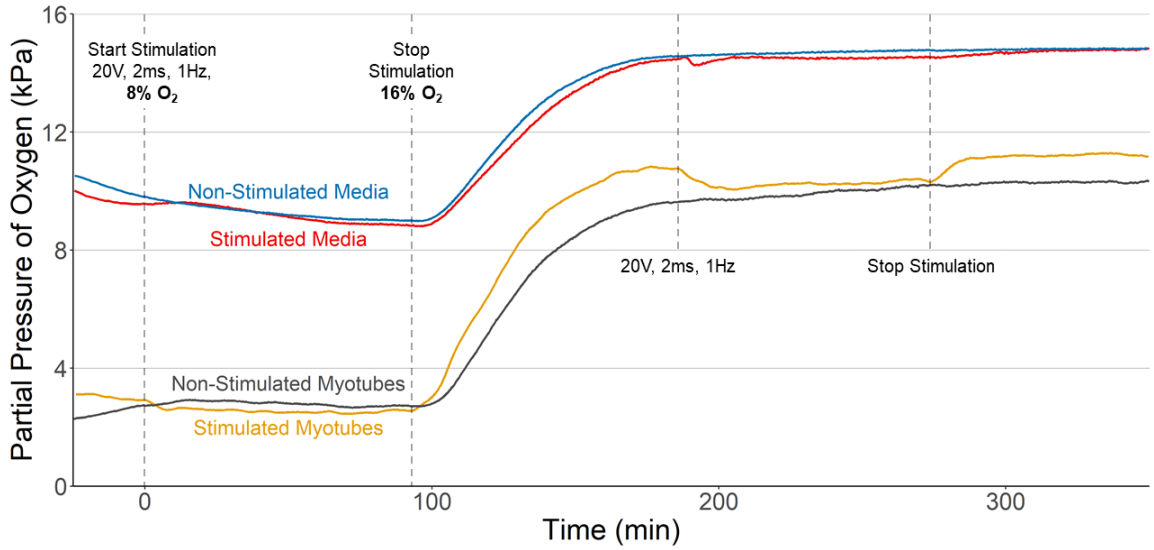

Figure 3.15 Oxygen partial pressure kinetics of contracting C_2C_{12} myotubes in8% and 16% O_2 atmospheres

Partial pressures of oxygen were measured in the culture media of dishes with and without cultured C_2C_{12} myotubes and with and without EPS (20 V, 2 ms, 1 Hz). The atmospheric oxygen was set to 8% and EPS was applied for 90 minutes. The stimulation was stopped and the atmospheric O_2 was changed to 16%. After 90 minutes of equilibration, EPS was applied for another 90 minutes.

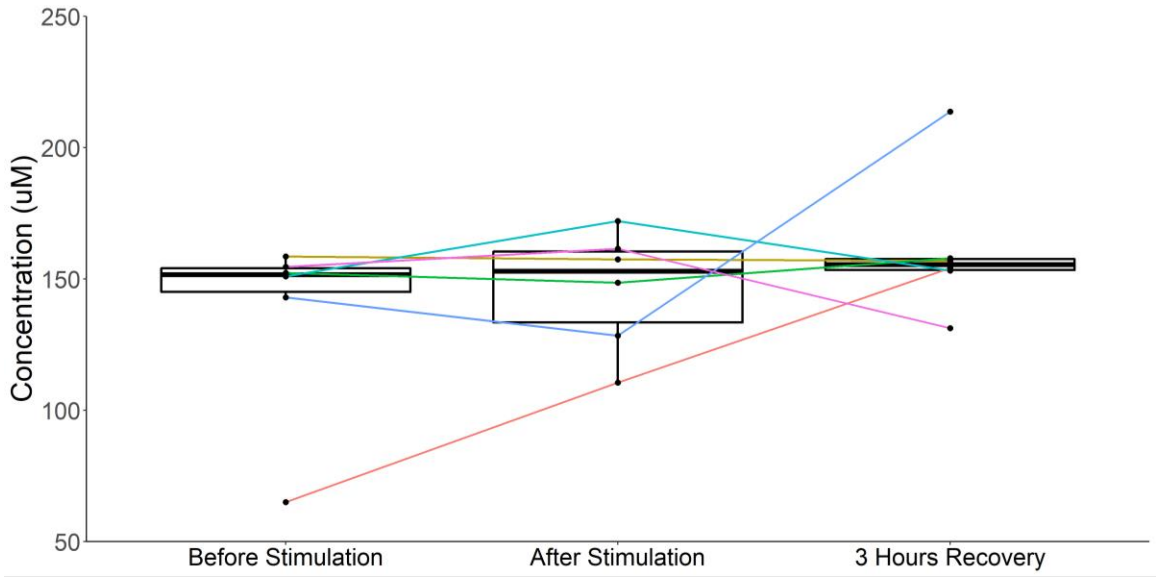

Figure 3.16 Intracellular ATP concentration of C_2C_{12} myotubes in response to electrical stimulation

C_2C_{12} myotubes were frozen at time = 0, 180, and 360 of the time course experiment outlined in Figure 3.18. The black points represent the raw data from six independent biological replicates. The colored lines connect the data from a given replicate. No statistical difference was detected at any of the time points (p = 0.389).

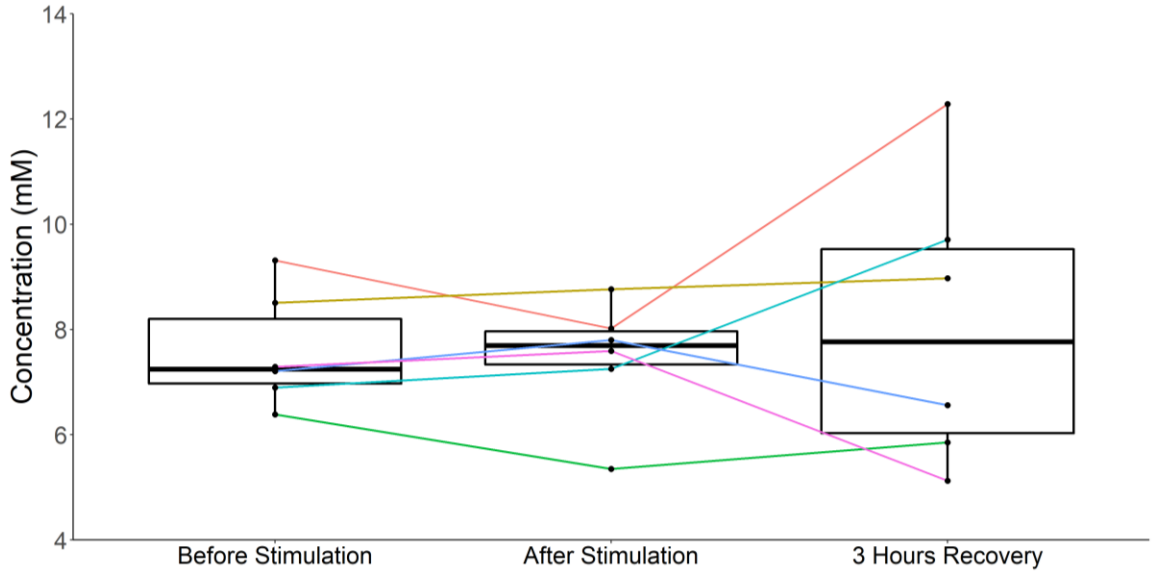

Figure 3.17 Concentration of secreted L-lactate from C_2C_{12} myotubes in response to electrical stimulation

Cell culture media from C_2C_{12} myotubes were frozen at time = 0, 180, and 360 of the time course experiment outlined in Figure 3.18. The black points represent the raw data from six independent biological replicates. The colored lines connect the data from a given replicate. No statistical difference was detected at any of the time points (p = 0.903).

3.6. EPS increases AMPK signaling

To investigate whether myotube contraction enhances AMPK signaling, I electrically stimulated C_2C_{12} myotubes for 180 minutes at 20 V, 2 ms, and 1 Hz and sampled cells at various time points during and post-stimulation (Figure 3.18). Additionally, I sampled resting myotubes before and after stimulation, and after three hours of recovery to serve as controls. Six biological replicates of the time course were performed using cells from the same lot, but each from different frozen stocks.

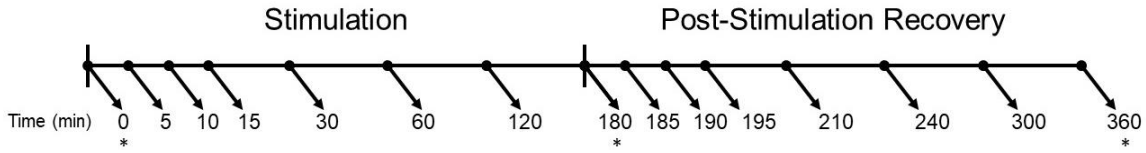

Figure 3.18 Time course experiment design
C_2C_{12} myotubes differentiated for five days were electrically stimulated (20 V, 2 ms, 1 Hz) for 180 minutes followed by 180 minutes of recovery. Cells were frozen at the indicated time points (minutes). * denotes the collection of media. Resting myotubes served as controls and were frozen at 0, 180, and 360 min.

After 180 minutes of electrical stimulation, p-AMPK, p-ACC, and p-TBC1D1 levels increased 1.24- ($p = 0.85$), 2.41- ($p = 0.004$), and 1.33-fold ($p = 0.029$), respectively, compared to pre-stimulation (Figure 3.19). After three hours of recovery, p-AMPK, p-ACC, and p-TBC1D1 levels increased 1.68- ($p = 0.57$), 2.71- ($p = 0.025$), and 1.11-fold ($p = 0.94$), respectively, compared to pre-stimulation (Figure 3.19).

The more detailed time courses revealed that levels of p-ACC and p-TBC1D1 reached a maximum of 2.7- and 1.36-fold increase after 120 minutes of stimulation, respectively, compared to levels measured at 0 min. (Figure 3.20). Levels of p-AMPK initially decreased 0.84-fold after five minutes of stimulation and reached a maximum of 1.47-fold after 120 minutes of stimulation. Stopping stimulation led to immediate decreases in p-AMPK, p-ACC, and p-TBC1D1 levels of 0.29-, 0.64-, and 0.27-fold, respectively, compared to their signals at 180 min (Figure 3.20). These decreases were then followed by increased levels of p-AMPK, p-ACC, and p-TBC1D1 after 120 minutes of recovery. After three hours of recovery from EPS, p-AMPK, p-ACC, and p-TBC1D1 were increased compared to before stimulation.

In response to the same bout of EPS, total AMPK, ACC, and TBC1D1 reached a maximum of 1.39-, 1.17-, and 1.59-fold increase after 180, 120, and 30 minutes of

stimulation, respectively. (Figure 3.21). Stopping stimulation resulted in varying acute signaling of the three molecules: AMPK decreased 0.16-fold and then increased 0.05-fold, ACC increased 0.19-fold, and TBC1D1 decreased 0.24-fold and then increased 0.04-fold.

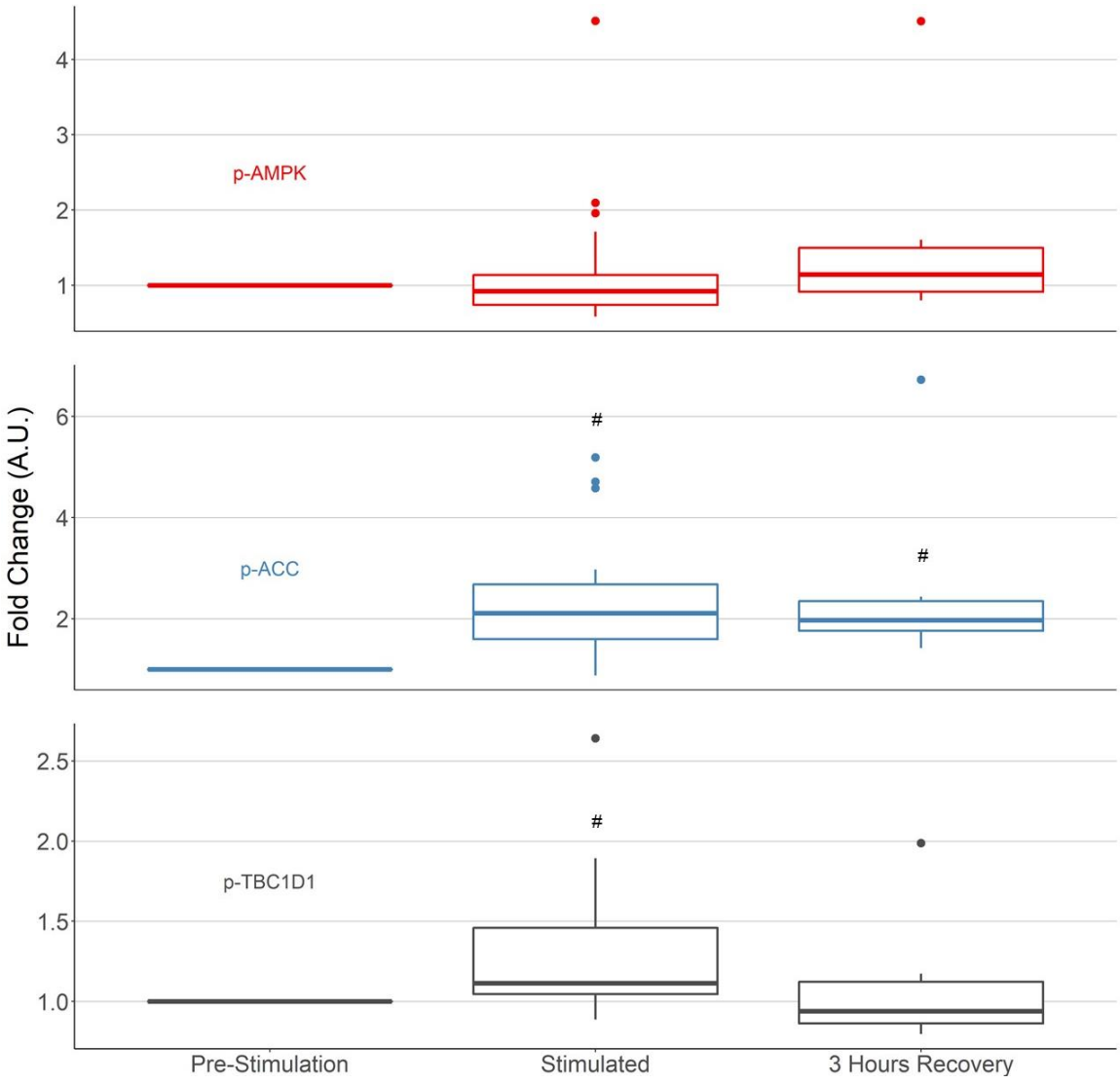

Figure 3.19 AMPK signaling of C_2C_{12} myotubes after three hours of electrical stimulation followed by three hours of recovery

C_2C_{12} myotubes differentiated for five days were electrically stimulated (20 V, 2 ms, 1 Hz) for 180 minutes followed by 180 minutes of recovery. Cell lysates were subjected to immunoblotting and levels of p-AMPK, p-ACC, and p-TBC1D1 were quantified by densitometry. Six biological replicates were performed. Pre-stimulation represents time point = 0 (n = 6/molecule). Stimulated represents the mean of time points 60, 120, and 180 for each molecule (n = 18). 3 hours recovery represents time point = 360 (n = 6). # denotes $p < 0.05$ compared to pre-stimulation. A. U. = arbitrary units.

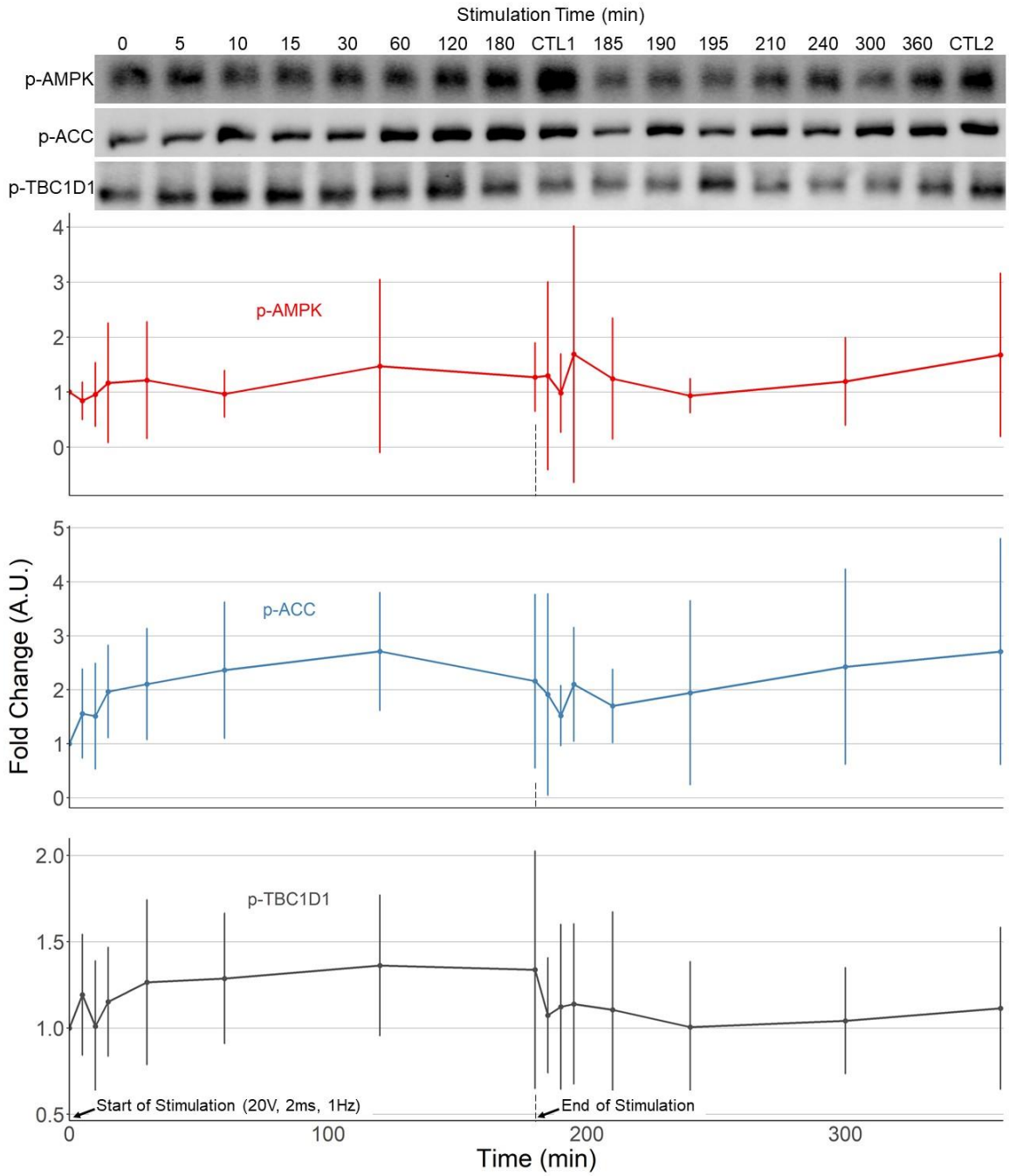

Figure 3.20 Time course of AMPK signaling of C_2C_{12} myotubes during three hours of electrical stimulation followed by three hours of recovery

C_2C_{12} myotubes differentiated for five days were electrically stimulated (20 V, 2 ms, 1 Hz) for 180 minutes followed by 180 minutes of recovery. Cell lysates were subjected to immunoblotting and levels of p-AMPK, p-ACC, and p-TBC1D1 were quantified by densitometry. Data points represent the mean of six biological replicates and the error bars represent 95% confidence intervals. Images from representative immunoblots for p-AMPK, p-ACC, and p-TBC1D1 are shown at the top. CTL1 = resting myotubes sampled at 180 minutes. CTL2 = resting myotubes sampled at 360 minutes. A. U. = arbitrary units.

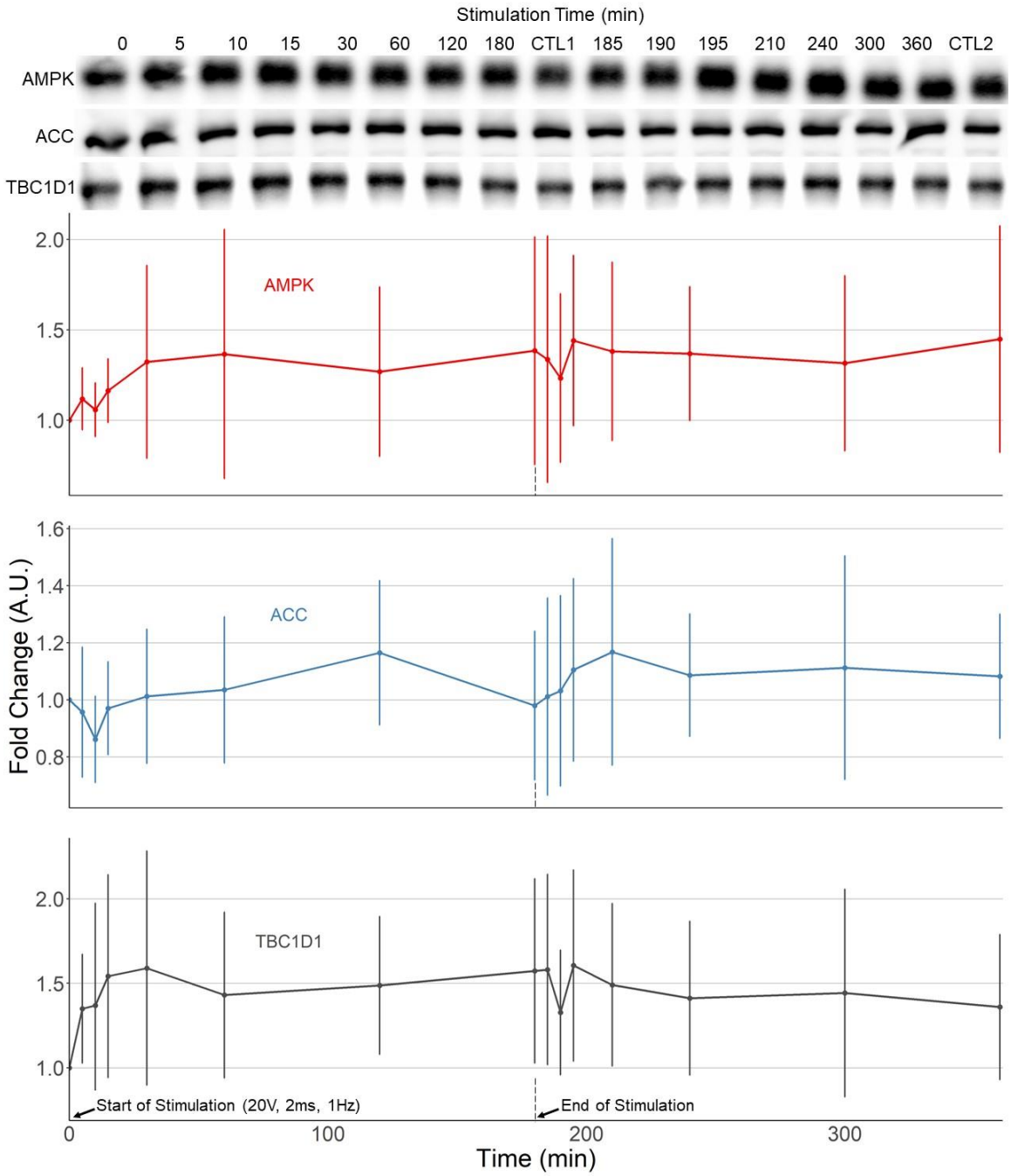

Figure 3.21 Time course of total AMPK, ACC, and TBC1D1 of C_2C_{12} myotubes during three hours of electrical stimulation followed by three hours of recovery

C_2C_{12} myotubes differentiated for five days were electrically stimulated (20 V, 2 ms, 1 Hz) for 180 minutes followed by 180 minutes of recovery. Cell lysates were subjected to immunoblotting and levels of AMPK, ACC, and TBC1D1 were quantified by densitometry. Data points represent the mean of six biological replicates and the error bars represent 95% confidence intervals. Images from representative immunoblots for AMPK, ACC, and TBC1D1 are shown at the top. CTL1 = resting myotubes sampled at 180 minutes. CTL2 = resting myotubes sampled at 360 minutes. A. U. = arbitrary units.

Normalizing the phospho-protein levels to the respective total protein levels demonstrates that AMPK and TBC1D1 phosphorylation occurs to a lesser extent (1.01- and 0.93- fold, respectively) compared to ACC phosphorylation (2.24-fold) in response to three hours of electrical stimulation (Figure 3.22).

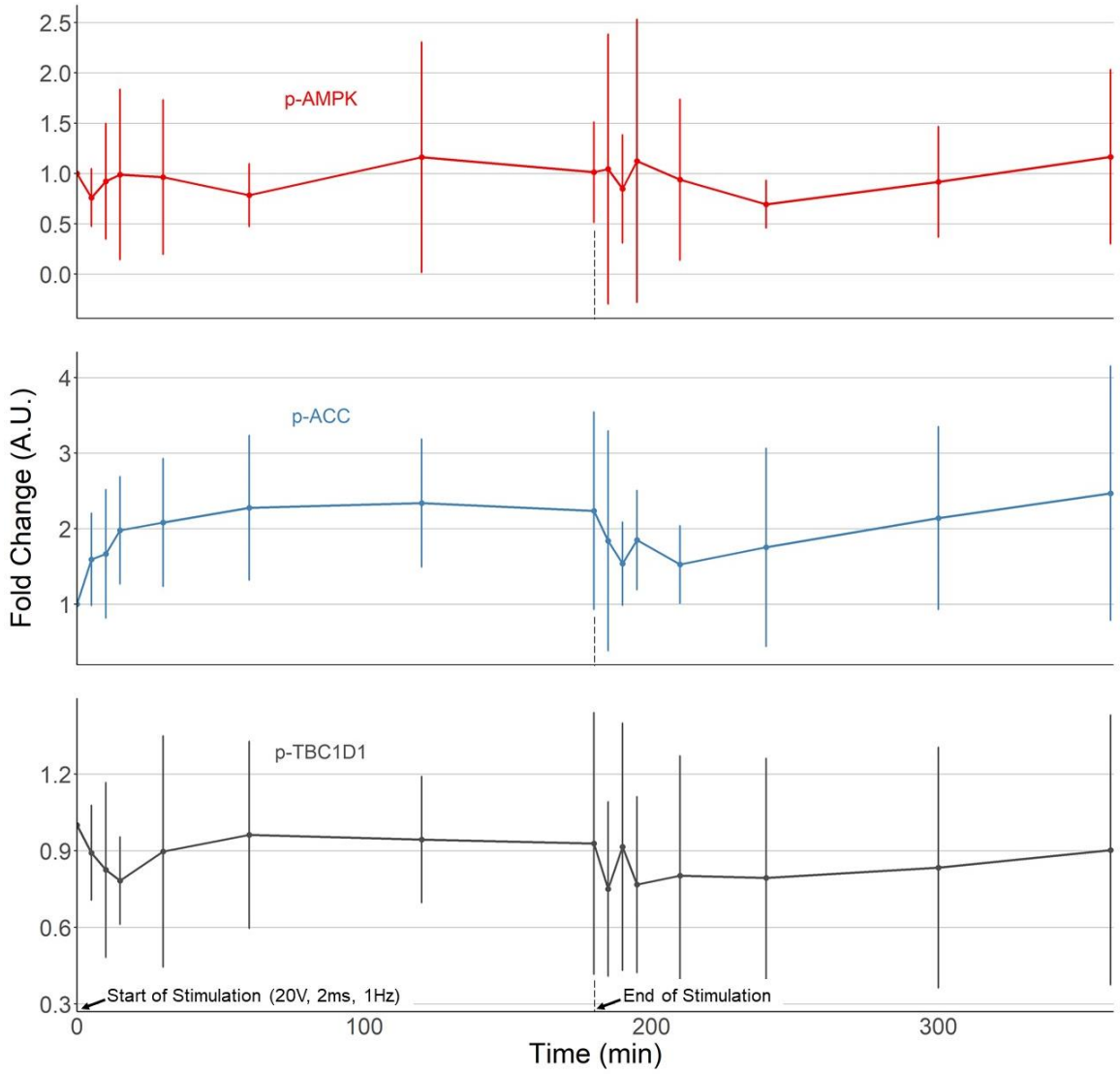

Figure 3.22 Time course of AMPK signaling normalized to total protein of C_2C_{12} myotubes during three hours of electrical stimulation followed by three hours of recovery

Normalized fold changes of phospho-protein to total protein were calculated from the data in Figure 3.20 and Figure 3.21. A. U. = arbitrary units.

The stimulation experiments present three possible confounds: 1) AMPK signaling could vary over time in resting myotubes due to factors other than EPS, 2) the presence of undifferentiated non-contractile myoblasts and 2) the presence of the electrodes being

in contact with the cell culture media. To ensure that EPS was responsible for the observed changes in signaling, I measured the levels of p-AMPK, p-ACC, and p-TBC1D1 in resting myotubes sampled before and after the stimulation period and again after the recovery period. Phospho-levels for each protein were not statistically different from each other between the time points (p = 0.5) (Figure 3.23).

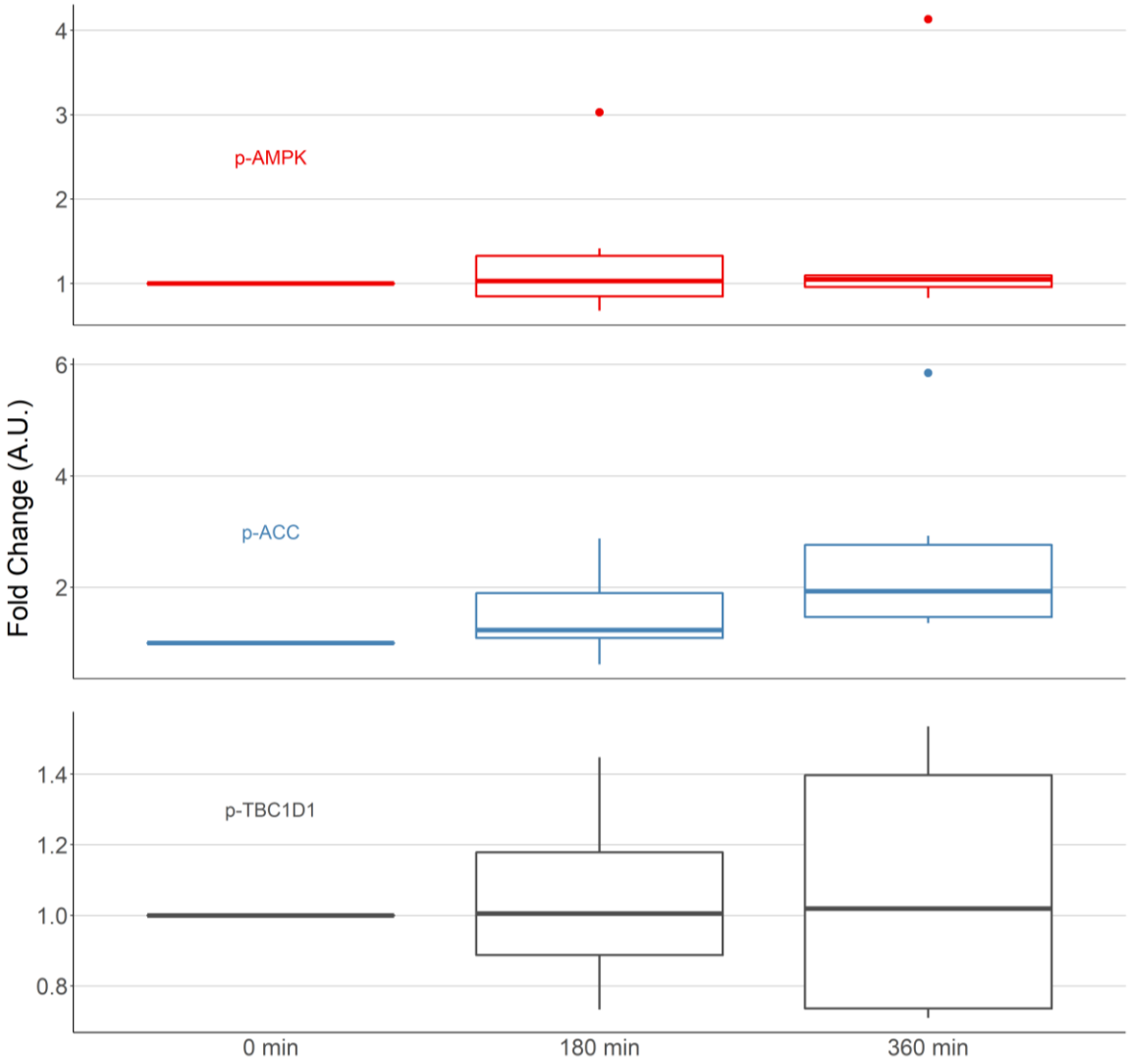

Figure 3.23 AMPK signaling of resting C_2C_{12} myotubes throughout the time course experiment

Resting C_2C_{12} myotubes serving as controls for the time course experiment outlined in Figure 3.18 were frozen at time = 0, 180, and 360. Cell lysates were subjected to immunoblotting and levels of p-AMPK, p-ACC, and p-TBC1D1 were quantified by densitometry. Raw data of six biological replicates presented. None of the proteins exhibited statistically significant different levels between the time points. A. U. = arbitrary units.

To test whether myoblasts exhibit an AMPK response to electrical stimulation, C_2C_{12} myoblasts were stimulated alongside the myotubes in the time course experiment outlined in Figure 3.18 and sampled at 0, 180, and 360 min. Figure 3.24 illustrates AMPK signaling for pre- and post-stimulation of myotubes, a positive control (EPS + 2 mM AICAR + 100 µM A-769662), an electrode immersion control, and the AMPK signaling of myoblasts throughout EPS. Electrical stimulation did not affect myoblast AMPK signaling ($p > 0.18$, Figure 3.24). Finally, AMPK signaling was not increased when electrodes were incubated with myotubes without EPS being applied ($p > 0.06$, Figure 3.24).

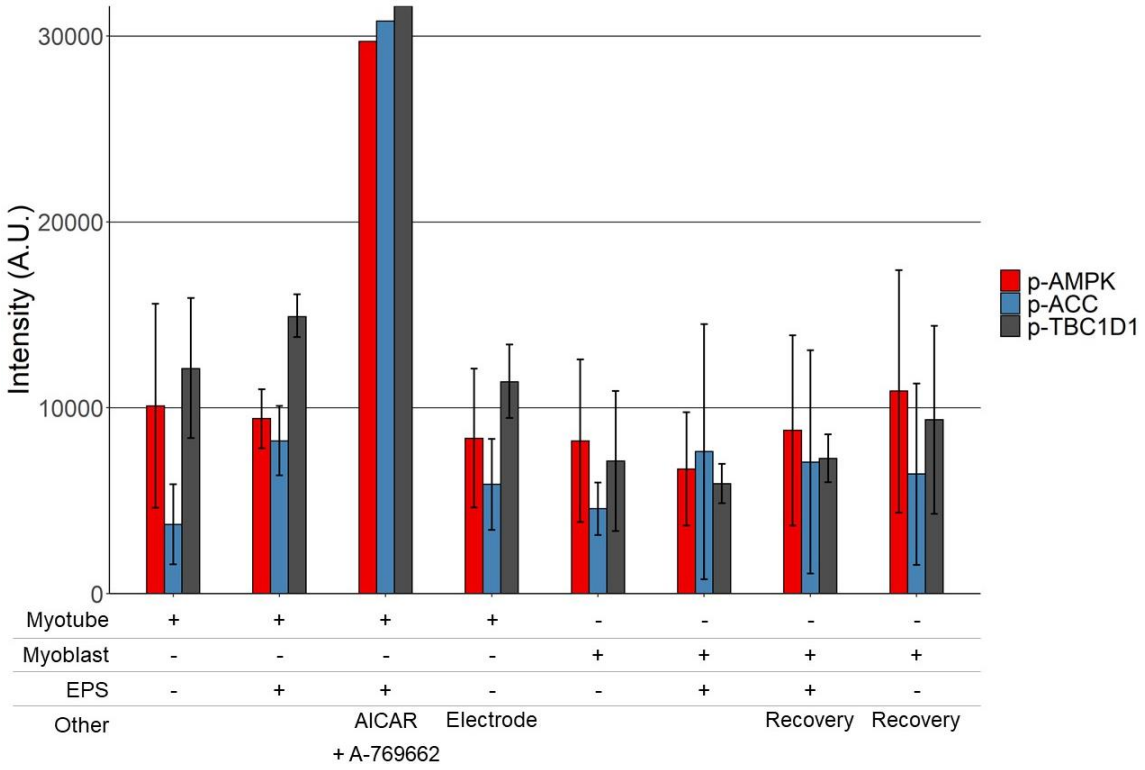

Figure 3.24 AMPK signaling of various control conditions during electrical stimulation of C_2C_{12} myotubes

C_2C_{12} myotubes differentiated for five days and ~80% confluent C_2C_{12} myoblasts were used for various controls during the time course experiment outlined in Figure 3.18. Cell lysates were subjected to immunoblotting and levels of p-AMPK, p-ACC, and p-TBC1D1 were quantified by densitometry. EPS = Electrical pulse stimulation (20 V, 2 ms, 1 Hz). Recovery = EPS + three hours of recovery. Where indicated, AICAR (2 mM) and A-769662 (100 µM) were incubated for 30 minutes. Electrode = electrodes immersed in culture media. Data represent the mean of six biological replicates ± 95% confidence intervals (except AICAR treatment condition which is from one experiment). A.U. = arbitrary units.

3.7. EPS did not damage the myotubes

Live-cell imaging revealed no disruption in the contractile ability of C_2C_{12} myotubes throughout the three-hour stimulation. To further investigate whether EPS resulted in cytotoxicity, I measured LDH levels from the media of stimulated C_2C_{12} myotubes collected before, immediately after and three hours after stimulation (Figure 3.18). The premise of this experiment is that LDH is not normally secreted from healthy cells but damage to the cell membrane would allow LDH to leak into the cell culture media [121]. Three hours of electrical stimulation did not increase LDH in the media compared to before stimulation (Figure 3.25).

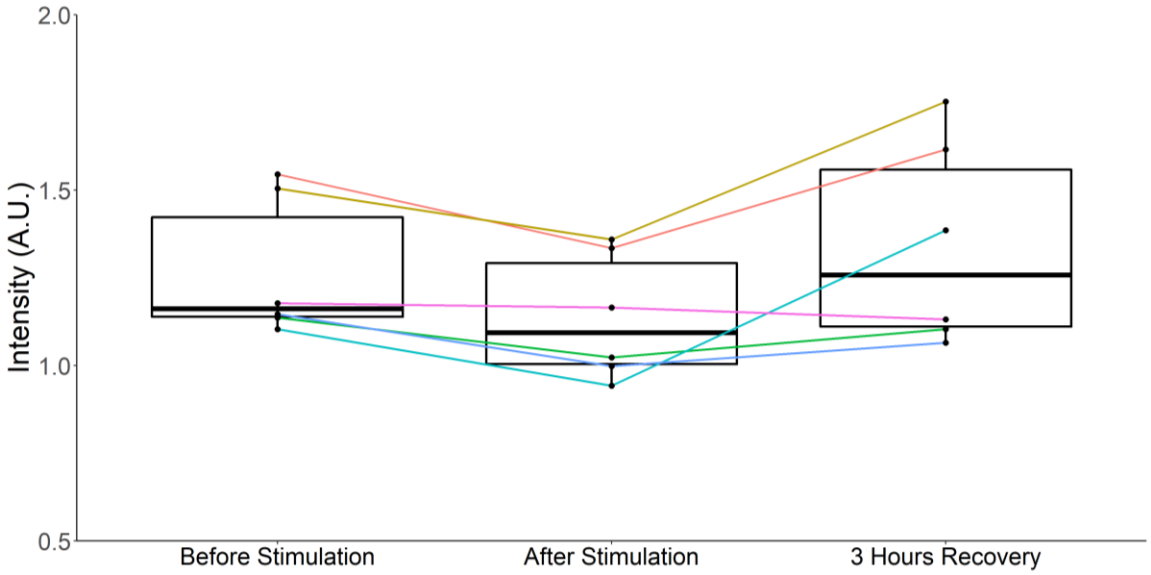

Figure 3.25 LDH levels in cell culture media of C_2C_{12} myotubes in response to electrical stimulation

Cell culture media from C_2C_{12} myotubes were frozen at 0, 180, and 360 min of the time course experiment outlined in Figure 3.18. The black points represent the raw data from six independent biological replicates. The colored lines connect the data from a given replicate. A. U. = arbitrary units.

3.8. Increasing frequency of electrical stimulation led to further decreases in pO_2 in a 16% but not a 4% O_2 atmosphere

The marginal activation of AMPK demonstrated in the time course experiment, as well as the non-differences observed in other experiments within the thesis, prompted me

to test whether more intense electrical stimulation could result in enhanced AMPK signaling. To ascertain stimulation conditions that were more metabolically stressful, I tested the effect of increased stimulation frequency on O_2 consumption. Specifically, I measured the pO_2 of the media of contracting myotubes in response to stimulation at 1, 2, 4, and 6 Hz (20 V, 2 ms). Additionally, I tested each of the stimulation frequencies in a 16% and 4% O_2 atmosphere.

The 16% O_2 atmosphere resulted in steady state pO_2 of approximately 9 kPa in the cell culture media of myotubes. The pO_2 of cell culture media of contracting myotubes with a stimulation frequency of 1, 2, 4, and 6 Hz in a 16% O_2 atmosphere decreased by 0.53, 1.74, 2.17, and 1.83 kPa, respectively, compared to before starting the corresponding bout of stimulation (Figure 3.26, yellow line). In contrast, the pO_2 of cell culture media overlying non-stimulated myotubes was only slightly affected (Figure 3.26, black line). Stimulation frequencies of 1 and 2 Hz did not affect the stimulated cell culture media; however, stimulation frequencies of 4 and 6 Hz caused marked reductions in the measured pO_2 (Figure 3.26, red line). The effect of decreased pO_2 in cell culture media alone in response to high stimulation frequencies was exaggerated at 60 Hz (data not shown).

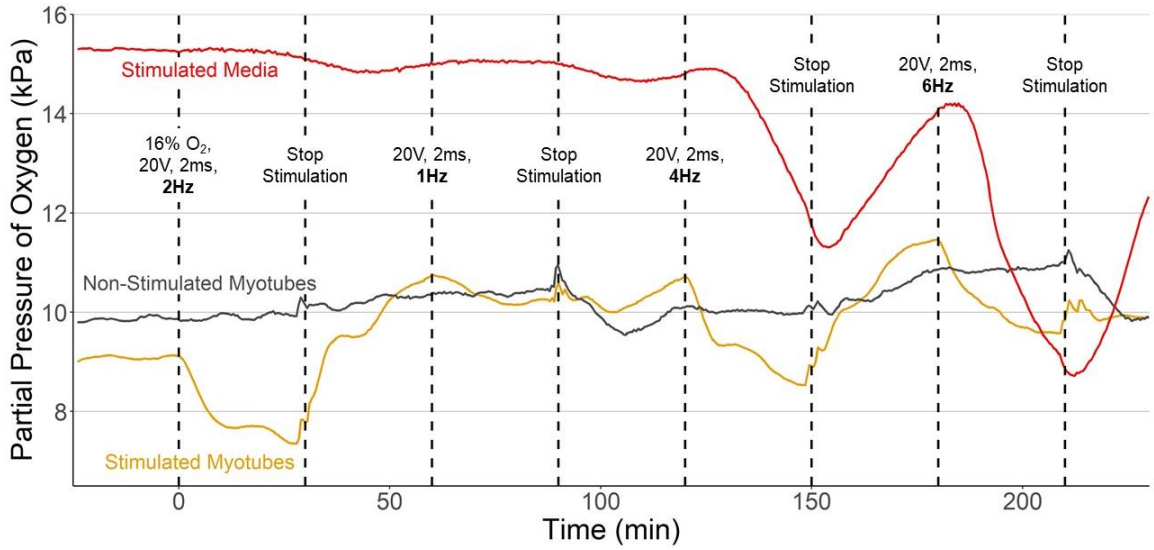

Figure 3.26 Oxygen partial pressure kinetics in response to various frequencies in a 16% O_2 atmosphere

C_2C_{12} myotubes were electrically stimulated (20 V, 2 ms) at four different frequencies (1, 2, 4, and 6 Hz) in a 4% O_2 atmosphere for 30 minutes followed by 30 minutes of recovery. Data are from a single experiment.

The 4% O_2 atmosphere resulted in steady state pO_2 of approximately 0.02 – 0.5 kPa in the cell culture media of myotubes. The pO_2 of cell culture media of contracting

myotubes in the 4% O_2 atmosphere decreased, however, the equilibrated pO_2 of the stimulated myotubes (0.02 kPa) did not allow for large decreases in the pO_2 (Figure 3.27, yellow line), therefore the magnitude of change in response to increasing stimulation frequency could not be accurately measured (Figure 3.28). The pO_2 of cell culture media of non-stimulated myotubes increased after stopping the first bout of stimulation (Figure 3.27, black line). Lastly, none of the stimulation frequencies affected the stimulated cell culture media at 4% O_2 (Figure 3.27, red line).

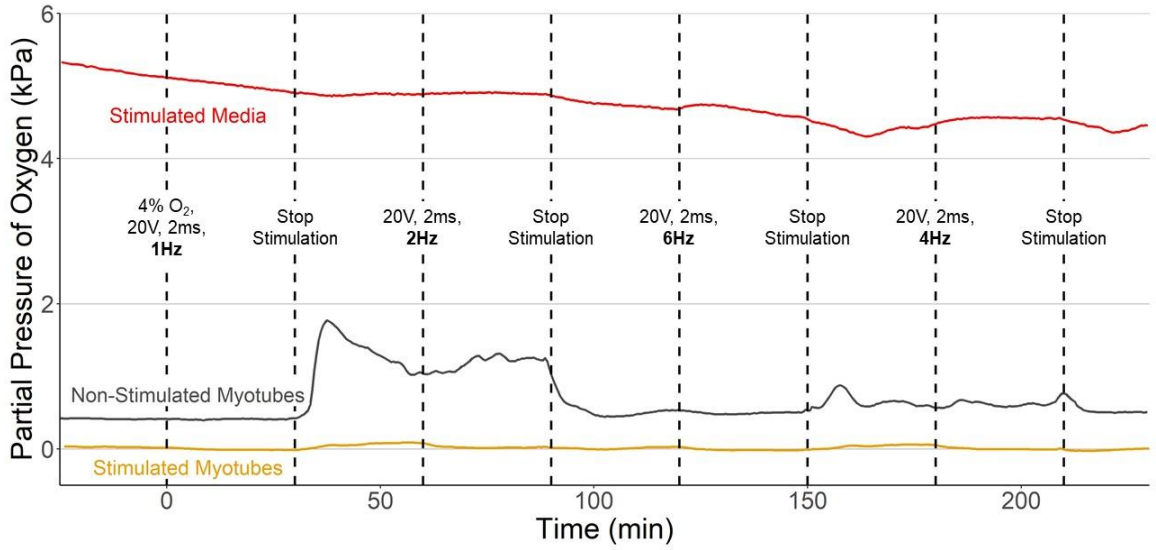

Figure 3.27 Oxygen partial pressure kinetics in response to various frequencies in a 4% O_2 atmosphere

C_2C_{12} myotubes were electrically stimulated (20 V, 2 ms) at four different frequencies (1, 2, 4, and 6 Hz) in a 4% O_2 atmosphere for 30 minutes followed by 30 minutes of recovery. Data are from a single experiment.

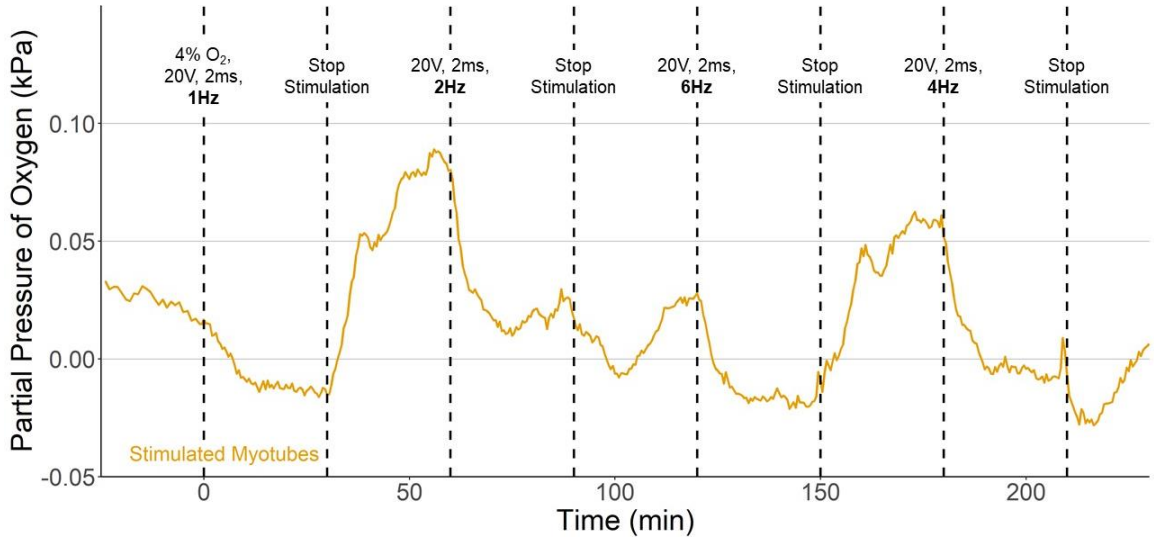

Figure 3.28 Oxygen partial pressure kinetics in response to various frequencies in a 4% O_2 atmosphere (enlargement of Figure 3.27)

C_2C_{12} myotubes were electrically stimulated (20 V, 2 ms) at four different frequencies (1, 2, 4, and 6 Hz) in a 4% O_2 atmosphere for 30 minutes followed by 30 minutes of recovery. Data are from a single experiment.

Lastly, to confirm that low stimulation frequencies (1 and 2 Hz) did not result in a decreased pO_2 in cell culture media alone, I stimulated (20 V, 2 ms) C_2C_{12} myotubes differentiated for five days in an 8% O_2 atmosphere at 1 and 2 Hz. Figure 3.29 illustrates that the pO_2 in cell culture media alone was not affected by low stimulation frequencies, but that the stimulated myotubes were.

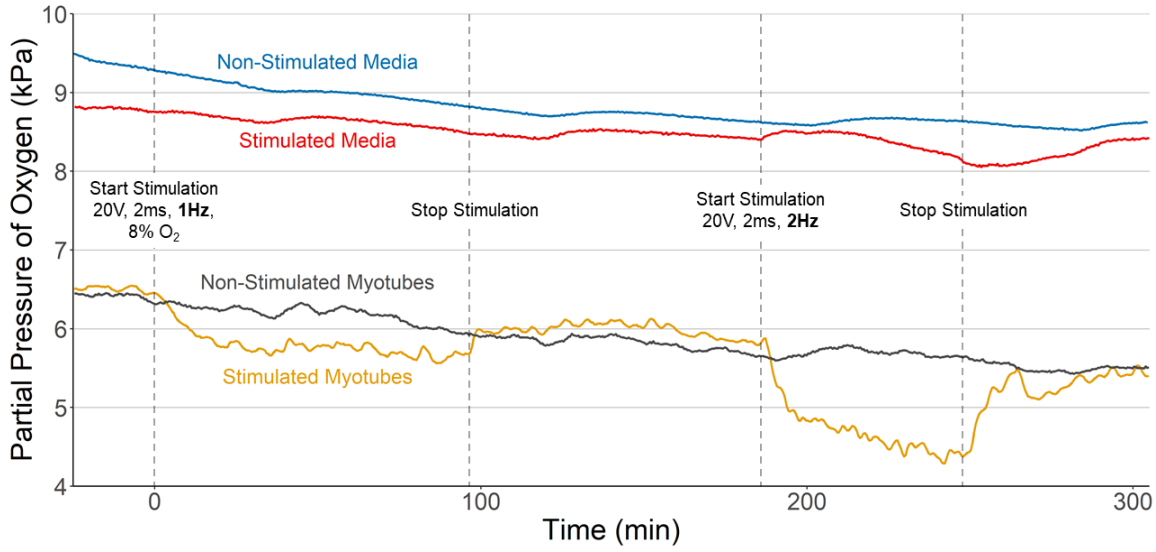

Figure 3.29 Oxygen partial pressure kinetics in response to 1 and 2 Hz stimulation frequency

Partial pressure of oxygen of cell culture media with and without cultured C_2C_{12} myotubes, and with and without EPS (20 V, 2 ms). Atmospheric oxygen was set to 8% and EPS (1 Hz) was applied for 90 minutes at time = 0. After 90 minutes of recovery, EPS (2 Hz) was applied for 70 minutes at time = 180. Data are from a single experiment.

Figure 3.30 illustrates changes in AMPK signaling and HIF1α accumulation resulting from increased stimulation frequency in a 16% and 4% O_2 atmosphere. Compared to resting myotubes, treatment with 2 mM AICAR increased AMPK signaling in both atmospheric conditions but increasing stimulation frequency did not. HIF1α accumulation increased in the 4% but not the 16% O_2 atmosphere. Lastly, increasing stimulation frequency in both O_2 atmospheres did not result in more HIF1α accumulation (Figure 3.30).

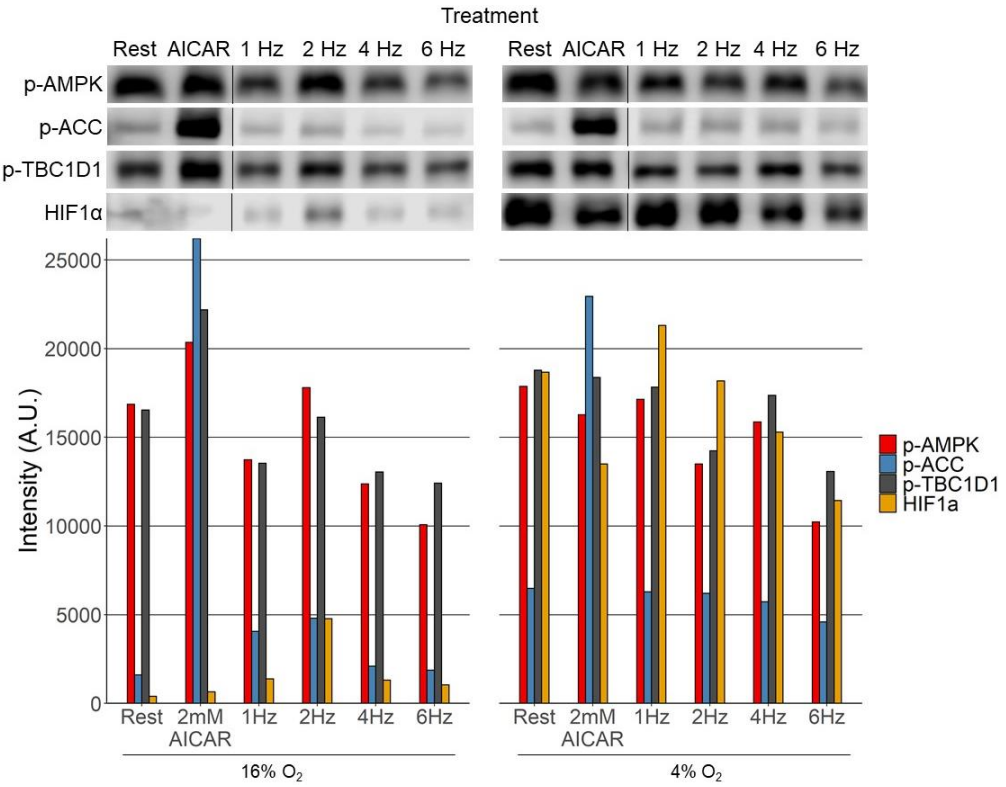

Figure 3.30 AMPK signaling and HIF1α accumulation in response to increasing stimulation frequencies in a 16% and 4% O_2 atmosphere

C_2C_{12} myotubes were electrically stimulated (20 V, 2 ms) at four different frequencies (1, 2, 4, and 6 Hz) in a 16% and 4% O_2 atmosphere for 30 minutes. For AICAR treatment, C_2C_{12} myotubes were incubated with AICAR (2 mM) for 30 minutes. The immunoblots for p-AMPK, p-ACC, p-TBC1D1, and HIF1α are shown at the top. Data are from a single experiment. A.U. = arbitrary units.

Chapter 4. Discussion

Exercise is a potent activator of AMPK in skeletal muscle. AMPK activity during and after exercise is thought to be important for adaptation; however, the importance of AMPK signaling over time (AMPK dynamics) to coordinating fitness-promoting adaptations remains poorly understood. To better understand the role of AMPK activity in coordinating adaptation, the time course of AMPK activity during and after exercise must first be investigated.

The aim of this thesis was to develop and evaluate electrical stimulation of C_2C_{12} myotubes as an in vitro model of exercise to study AMPK dynamics. In the present study, I demonstrated that differentiation of C_2C_{12} myoblasts resulted in contractile myotubes. Moreover, I showed that AMPK signaling was both observable in electrically stimulated C_2C_{12} myotubes and that it could be induced and repressed using small molecules. Additionally, I showed that electrical stimulation resulted in a decreased partial pressure of oxygen (pO_2) in the media of contracting myotubes. Lastly, I showed that three hours of electrical stimulation followed by three hours of recovery resulted in a dynamic AMPK response. Overall, these results support my hypotheses that the C_2C_{12} EPS model can be used to elicit exercise-like AMPK signaling, and that this signaling can be manipulated using small molecules. However, the AMPK signaling response was limited compared to the observed response in human muscle during exercise. More work is therefore necessary to define conditions that lead to a more robust AMPK signaling response.

4.1. Validation of using C_2C_{12} myotubes to study AMPK signaling

I first confirmed that I could differentiate C_2C_{12} myoblasts into myotubes. I observed a generally positive relationship between myotube density (pixels ≤ 75) and the number of differentiation days (Figure 3.3). The increased myotube density at day -2 and the decreased myotube density at day 5 are most likely due to inconsistencies in the image settings when the image was captured. I then confirmed the contractile ability of the differentiated myotubes. The contractile ability of the C_2C_{12} myotubes observed in this study was similar to that observed in video footage from other published studies [61, 122, 123]. However, many undifferentiated myoblasts remained in the dish and were present

during the experiments. Overall, these data suggest that the differentiation protocol produced contractile myotubes; however, further optimization may be possible.

One possible strategy to improve the differentiation protocol is to extend the protocol beyond five days. However, I observed by visual inspection that myotubes differentiated for more than six days exhibited morphologies that indicated potential damage, suggesting that an upper limit may exist to the number of days of differentiation. The potential detrimental effects of prolonged differentiation may be attenuated by switching the differentiation media to DMEM supplemented with 10% horse serum after five days of differentiation (P. Sobolewski, personal communication).

Next, I established that AMPK signaling could be manipulated in C_2C_{12} myotubes using small-molecule activators and inhibitors. The commonly used AMPK activator, AICAR, led to greater increases in AMPK signaling compared to the more specific activator, A-769662 (Figure 3.9). However, EPS combined with AICAR and A-769662 led to the greatest increase in AMPK signaling. Inhibiting AMPK signaling was achieved most effectively by compound C. Although p-TBC1D1 levels remained stable in response to increasing concentrations of compound C, treatment of C_2C_{12} myotubes with increasing concentrations of SBI-0206965 led to decreased levels of p-ACC and p-TBC1D1 but resulted in increasing levels of p-AMPK. Increasing levels of p-AMPK with an 'AMPK inhibitor' may produce conflicting signals at the molecular level that could result in discrepancies when interpreting data. Ultimately, using compound C and SBI-0206965 together could result in a more potent AMPK inhibitor cocktail, although the off-target effects would be magnified. Importantly, these results highlight treatments for positive and negative controls for future experiments.

Lastly, to verify that electrical stimulation metabolically perturbs the myotubes, I used optical oxygen sensor technology that allows for real-time oxygen measurement within the C_2C_{12} EPS model. In response to electrical stimulation, the pO_2 of cell culture media of C_2C_{12} myotubes decreased (Figure 3.14, Figure 3.15, and Figure 3.26). The decrease in the pO_2 was observed in response to different stimulation frequencies (1, 2, 4, and 6 Hz) and in 16%, 8%, and 4% O_2 atmospheres (Figure 3.14, Figure 3.26, and Figure 3.27). In general, increasing stimulation frequency resulted in larger decreases in the pO_2, suggesting that increasing stimulation frequency increases cellular respiration,

thus indicating enhanced metabolic stress. Together, these data indicate that electrical stimulation of differentiated C_2C_{12} myotubes can be used to study AMPK in a dish.

Mouse C_2C_{12} and primary human myotubes are widely used in in vitro models of skeletal muscle, however, the two cell lines exhibit differences in their bioenergetics [124, 125]. The bioenergetic differences manifest as preferential use of substrates and their corresponding metabolic pathways. Both human and C_2C_{12} myotubes express high levels of mRNA associated with contractile protein activity, albeit lower than in mature adult tissue [124]. Compared to primary human myotubes, C_2C_{12} myotubes exhibit higher expression of type II myosin heavy chain, which is associated with type II (fast-twitch, glycolytic) fibers, yet they exhibit higher oxygen consumption rates compared to human myotubes [124]. In addition, C_2C_{12} myotubes exhibit increased glucose uptake in response to EPS compared to primary human myotubes [124] but similar fatty acid oxidation. In this regard, the metabolic behaviours of human and C_2C_{12} myotubes may potentiate different metabolic effects under similar experimental conditions.

4.2. AMPK signaling in response to electrical stimulation

The AMPK response to electrical stimulation observed in this study was less robust than that reported by other groups [60-62]. In contrast to these data, I observed no increase in AMPK phosphorylation and only marginal increases in ACC and TBC1D1 phosphorylation by comparison to other studies. Specifically, Nedachi [60] demonstrated that after 24 hours of low frequency electrical stimulation of C_2C_{12} myotubes, p-AMPK and p-ACC increased approximately 4-fold. Additionally, Li [62] demonstrated that 60 minutes of low frequency electrical stimulation resulted in a 2.5-fold increase in p-AMPK and p-ACC. Additionally, data from human experiments demonstrate that in response to 30 minutes of moderate-intensity exercise, AMPK signaling increased ~3-fold and ACC phosphorylation increased 36-fold [53]. Overall, the marginal increase in AMPK signaling observed in this study may reflect normal physiology; however, more data are needed to corroborate this supposition.

The lack of increase in p-AMPK and relatively low fold-changes in p-ACC and p-TBC1D1 following electrical stimulation prompted me to test whether increasing stimulation frequency and decreasing atmospheric O_2 could further increase AMPK signaling [126]. In previous experiments, increasing the stimulation voltage did not result

in further decreases in the pO_2 of contracting myotubes suggesting that increasing the voltage may not increase the metabolic demand of the myotubes. Additionally, pulse durations used in neuromuscular electrical stimulation in vivo are most commonly 50 to 1000 µs [127], suggesting that minimal pulse durations should be used if the goal is to mimic human physiology. Moreover, the stimulation voltage and pulse duration define the threshold for initiating contraction and muscle fiber recruitment whereas the stimulation frequency grades the degree of contraction from multiple twitches to fused tetanus, as well as the concomitant force [128, 129]. Therefore, I decided to vary the stimulation frequency in a high (16%) and low (4%) O_2 atmosphere.

Although electrical stimulation at 4% O_2 resulted in higher AMPK signaling compared to 16% O_2 in resting myotubes, no effect of decreasing atmospheric oxygen on AMPK signaling was observed in stimulated myotubes (Figure 3.30). Additionally, increasing stimulation frequency in both the 16% and 4% O_2 atmosphere did not increase AMPK signaling (Figure 3.30). To confirm that the cells were experiencing hypoxia in the 4% O_2 atmosphere, I measured the levels of hypoxia-inducible factor 1α (HIF1α) [130]. Figure 3.30 demonstrates accumulation of HIF1α in a 4% but not 16% O_2 atmosphere. This result indicates that a 4% O_2 atmosphere is sufficient to induce cellular hypoxia. Moving forward, attempts should be made to determine the atmospheric O_2 required to best mimic the pO_2 in vivo; however, hypoxia alone cannot be expected to enhance AMPK signaling.

4.3. Limitations

I propose three main limitations of this study. First, the selected electrical stimulation parameters were based on values reported in the literature [60, 70]. However, a lack of consensus exists as to what stimulation parameters ought to be used [70]. Therefore, the marginal AMPK signaling response that I observed was likely due to these parameters being insufficiently severe, especially in light of the unchanged ATP and lactate concentrations. At minimum, the protocol elicited increased aerobic metabolism, as demonstrated by the apparent consumption of oxygen during the stimulation. To determine the stimulation parameters (voltage, frequency, pulse duration, and time duration) required to elicit a greater AMPK response, I would perform a factorial experiment that covers the ranges of stimulation parameters found in the current literature. Moreover, intermittent protocols where high-intensity electrical stimulation is interspersed

with rest periods could also be tested [54, 74]. With the identification of stimulation parameters that elicit an exercise-like AMPK response, I would then seek to improve the model by incorporating hypoxia and temperature profiles that mimic those observed during exercise in vivo.

Second, all my data were obtained from C_2C_{12} cells, a murine cell line. We are ultimately interested in the AMPK response to exercise in human skeletal muscle. While human myotubes would provide more physiologically relevant data, C_2C_{12} myotubes provide a means to establish the system because of their extensive characterization in the literature. In addition, the results were obtained from a single lot of C_2C_{12} cells, such that the possibility exists that lot-specific responses may have been observed. I note, however, that most of the experiments in this thesis produced results that were consistent with previously published data, including for differentiation, contractility, and activator responsiveness. Unfortunately, investigators generally do not report the lot number of their cells in their published studies, which makes it challenging to evaluate the possibility of lot-specific responses. To address this possibility, I recommend performing validation experiments on C_2C_{12} cells from different lots to determine whether lot-specific responses occur.

Lastly, high stimulation frequencies (≥ 4 Hz) prompted an initial increase and then a large decrease in the pO_2 of cell culture media without cells. To my knowledge, this observation has never been reported but represents a confounding variable that could affect the physiology of the cells. The initial increase in the pO_2 at high stimulation frequencies can be explained by the oxygen gas produced by the electrolysis of water [131]. Indeed, I observed no increase in the pO_2 of de-ionized water in response to electrical stimulation (unpublished observations), which agrees with electrolysis being a contributing factor. The decline in the pO_2 following the increase, however, is more challenging to explain. Three possibilities exist: first, electrolysis can change the pH of a solution which in turn could affect the ability of the oxygen sensor to reliably report the pO_2 (IonOptix, personal communication). This hypothesis could be tested by titrating acid into cell culture media to determine if readings are affected by the altered pH. Second, phenol red is discouraged in fluorometry experiments (IonOptix, personal communication). Thirdly, electrolysis of water is endothermic thereby decreasing the temperature of the cell culture media. Because the optical oxygen sensors used in this study are temperature dependent, when the temperature decreases (such as in an endothermic reaction), the

pO_2 measurements will also decrease. Altogether, the apparent effect of the pO_2 in response to stimulation frequency is not obvious at low stimulation frequencies, however, if high stimulation frequencies are required, proper experimental controls must be included to account for this potential effect.

4.4. Future directions

Applying EPS to elicit exercise-like responses in cultured myotubes provides a promising tool to investigate the role of AMPK signaling in mediating skeletal muscle adaptations to exercise. To exploit this method, the electrical stimulation parameters needed to robustly activate AMPK signaling in an exercise-like manner must be determined. Subsequently, small-molecules inhibitors can be used to systematically block AMPK signaling during and after stimulation. Blocking AMPK signaling at various time points and studying how downstream adaptations are affected would provide insight into the role AMPK dynamics play in coordinating fitness-promoting adaptations. Lastly, the work presented in this thesis represents validation experiments required to extend the EPS model to human myotubes. Ultimately, using the EPS model with human myotubes to study the signaling network and dynamics at play during and after stimulation, we could investigate the molecular mechanisms underlying inter-individual differences in skeletal muscle adaptations to exercise [132, 133].

4.5. Conclusion

In this thesis, I showed that electrical stimulation of C_2C_{12} myotubes only marginally increased AMPK signaling. The magnitude of signaling was less than has been observed by others using similar models, less than the increases observed in human muscle during exercise, and less than the increases I observed in response to activator stimulation. The marginal signaling response was likely due to the stimulation parameters being insufficient to cause substantial increases in AMP and ADP. Overall, I conclude that electrical stimulation of C_2C_{12} myotubes is a promising means to study AMPK signaling dynamics but that more work is needed to define experimental conditions that better mimic exercise. Understanding the temporal dynamics of signaling in response to specific exercise protocols could enhance understanding of how signaling dynamics encode information

into skeletal muscle adaptation. This understanding could be applied to developing evidence-based approaches to personalized exercise programming.

References

1. Saklayen, M.G., *The Global Epidemic of the Metabolic Syndrome.* Current hypertension reports, 2018. **20**(2): p. 12-12.
2. Cartee, G.D., et al., *Exercise Promotes Healthy Aging of Skeletal Muscle.* Cell Metabolism, 2016. **23**(6): p. 1034-1047.
3. Gabriel, B.M. and J.R. Zierath, *The Limits of Exercise Physiology: From Performance to Health.* Cell Metabolism, 2017. **25**(5): p. 1000-1011.
4. Thompson, P.D., Crouse, S. F., Goodpaster, B., Kelley, D., Moyna, N., Pescatello, L., *The acute versus the chronic response to exercise.* Medicine & Science in Sports & Exercise, 2001. **33**(6): p. S438-S445.
5. Warburton, D.E.R., N. Gledhill, and A. Quinney, *Musculoskeletal Fitness and Health.* Canadian Journal of Applied Physiology, 2001. **26**(2): p. 217-237.
6. Warburton, D.E.R., N. Gledhill, and A. Quinney, *The Effects of Changes in Musculoskeletal Fitness on Health.* Canadian Journal of Applied Physiology, 2001. **26**(2): p. 161-216.
7. Warburton, D.E.R., C.W. Nicol, and S.S.D. Bredin, *Health benefits of physical activity: the evidence.* CMAJ : Canadian Medical Association Journal, 2006. **174**(6): p. 801-809.
8. Hoppeler, H., et al., *Molecular Mechanisms of Muscle Plasticity with Exercise*, in *Comprehensive Physiology*. 2011. p. 1383-1412.
9. Hoppeler, H., *Molecular networks in skeletal muscle plasticity.* Journal of Experimental Biology, 2016. **219**(2): p. 205-213.
10. Lim, W., Mayer, B., Pawson, T., *Cell Signaling: Principles and Mechanisms.* The Quarterly Review of Biology, 2017. **92**(1): p. 105-106.
11. Boggon, T.J. and M.J. Eck, *Structure and regulation of Src family kinases.* Oncogene, 2004. **23**(48): p. 7918-7927.
12. Martin, G.S., *The hunting of the Src.* Nature Reviews Molecular Cell Biology, 2001. **2**(6): p. 467-475.
13. Wang, Z. and P.A. Cole, *Catalytic mechanisms and regulation of protein kinases.* Methods in enzymology, 2014. **548**: p. 1-21.
14. Roskoski, R., *Enzyme Structure and Function*, in *Reference Module in Biomedical Sciences*. 2014, Elsevier.
15. Cohen, P., *The origins of protein phosphorylation.* Nature Cell Biology, 2002. **4**(5): p. E127-E130.
16. Wodak, S.J., et al., *Allostery in Its Many Disguises: From Theory to Applications.* Structure, 2019. **27**(4): p. 566-578.
17. Sharma, S.K. and R.M. Leblanc, *Biosensors based on β-galactosidase enzyme: Recent advances and perspectives.* Analytical Biochemistry, 2017. **535**: p. 1-11.
18. Kern, D. and E.R.P. Zuiderweg, *The role of dynamics in allosteric regulation.* Current Opinion in Structural Biology, 2003. **13**(6): p. 748-757.
19. Kenakin, T.P., *Chapter 7 - Allosteric Drug Antagonism*, in *A Pharmacology Primer (Third Edition)*, T.P. Kenakin, Editor. 2009, Academic Press: New York. p. 129-147.
20. Gowans, G.J., et al., *AMP is a true physiological regulator of AMP-activated protein kinase by both allosteric activation and enhancing net phosphorylation.* Cell metabolism, 2013. **18**(4): p. 556-566.

21. Ahalawat, N. and R.K. Murarka, *Molecular Mechanism of Nucleotide-Dependent Allosteric Regulation in AMP-Activated Protein Kinase.* The Journal of Physical Chemistry B, 2017. **121**(14): p. 2919-2930.
22. Hardie, D.G., F.A. Ross, and S.A. Hawley, *AMPK: a nutrient and energy sensor that maintains energy homeostasis.* Nature reviews. Molecular cell biology, 2012. **13**(4): p. 251.
23. Willows, R., et al., *Phosphorylation of AMPK by upstream kinases is required for activity in mammalian cells.* The Biochemical journal, 2017. **474**(17): p. 3059-3073.
24. Herzig, S. and R.J. Shaw, *AMPK: guardian of metabolism and mitochondrial homeostasis.* Nature reviews. Molecular cell biology, 2018. **19**(2): p. 121-135.
25. Thomson, D., *The role of AMPK in the regulation of skeletal muscle size, hypertrophy, and regeneration.* International journal of molecular sciences, 2018. **19**(10): p. 3125.
26. Mounier, R., et al., *Expanding roles for AMPK in skeletal muscle plasticity.* Trends in Endocrinology and Metabolism = Trends in Endocrinology & Metabolism, 2015. **26**(6): p. 275-286.
27. Hardie, D.G., *AMP-activated/SNF1 protein kinases: conserved guardians of cellular energy.* Nature Reviews Molecular Cell Biology, 2007. **8**(10): p. 774-785.
28. Richter, E.A. and N.B. Ruderman, *AMPK and the biochemistry of exercise: implications for human health and disease.* The Biochemical journal, 2009. **418**(2): p. 261-275.
29. Friedrichsen, M., et al., *Exercise-induced AMPK activity in skeletal muscle: Role in glucose uptake and insulin sensitivity.* Molecular and Cellular Endocrinology, 2013. **366**(2): p. 204-214.
30. O'Neill, H.M., et al., *AMP-activated protein kinase (AMPK) β1β2 muscle null mice reveal an essential role for AMPK in maintaining mitochondrial content and glucose uptake during exercise.* Proceedings of the National Academy of Sciences, 2011. **108**(38): p. 16092-16097.
31. Gaitanos, G.C., et al., *Human muscle metabolism during intermittent maximal exercise.* Journal of applied physiology, 1993. **75**(2): p. 712-719.
32. Hatakeyama, H., et al., *Cooperative actions of Tbc1d1 and AS160/Tbc1d4 in GLUT4-trafficking activities.* Journal of Biological Chemistry, 2019. **294**(4): p. 1161-1172.
33. Cartee, G.D., *Roles of TBC1D1 and TBC1D4 in insulin- and exercise-stimulated glucose transport of skeletal muscle.* Diabetologia, 2015. **58**(1): p. 19-30.
34. Zhang, H., et al., *AMPK activation serves a critical role in mitochondria quality control via modulating mitophagy in the heart under chronic hypoxia.* international journal of molecular medicine, 2018. **41**(1): p. 69-76.
35. Rabinovitch, R.C., et al., *AMPK Maintains Cellular Metabolic Homeostasis through Regulation of Mitochondrial Reactive Oxygen Species.* Cell Reports, 2017. **21**(1): p. 1-9.
36. Hardie, D.G., *AMP-activated protein kinase—an energy sensor that regulates all aspects of cell function.* Genes & development, 2011. **25**(18): p. 1895-1908.
37. Perry, C.G.R., et al., *Repeated transient mRNA bursts precede increases in transcriptional and mitochondrial proteins during training in human skeletal muscle.* The Journal of physiology, 2010. **588**(Pt 23): p. 4795-4810.
38. Hood, D.A., et al., *Maintenance of Skeletal Muscle Mitochondria in Health, Exercise, and Aging.* Annual Review of Physiology, 2019. **81**(1): p. 19-41.

39. Holloszy, J.O., *Biochemical Adaptations in Muscle: Effects of exercise on mitochondrial oxygen uptake and respiratory enzyme activity in skeletal muscle.* Journal of Biological Chemistry, 1967. **242**(9): p. 2278-2282.
40. Xu, Y., et al., *MicroRNA-761 regulates mitochondrial biogenesis in mouse skeletal muscle in response to exercise.* Biochemical and Biophysical Research Communications, 2015. **467**(1): p. 103-108.
41. Leary, S.C. and E.A. Shoubridge, *Mitochondrial biogenesis: Which part of "NO" do we understand?* BioEssays, 2003. **25**(6): p. 538-541.
42. Ploumi, C., I. Daskalaki, and N. Tavernarakis, *Mitochondrial biogenesis and clearance: a balancing act.* The FEBS journal, 2017. **284**(2): p. 183-195.
43. Jäger, S., et al., *AMP-activated protein kinase (AMPK) action in skeletal muscle via direct phosphorylation of PGC-1alpha.* Proceedings of the National Academy of Sciences of the United States of America, 2007. **104**(29): p. 12017-12022.
44. Bergeron, R., et al., *Chronic activation of AMP kinase results in NRF-1 activation and mitochondrial biogenesis.* American Journal of Physiology-Endocrinology and Metabolism, 2001. **281**(6): p. E1340-E1346.
45. Tanner, C.B., et al., *Mitochondrial and performance adaptations to exercise training in mice lacking skeletal muscle LKB1.* American journal of physiology. Endocrinology and metabolism, 2013. **305**(8): p. E1018-E1029.
46. Zong, H., et al., *AMP kinase is required for mitochondrial biogenesis in skeletal muscle in response to chronic energy deprivation.* Proceedings of the National Academy of Sciences of the United States of America, 2002. **99**(25): p. 15983-15987.
47. Garcia-Roves, P.M., et al., *Gain-of-function R225Q mutation in AMP-activated protein kinase γ3 subunit increases mitochondrial biogenesis in glycolytic skeletal muscle.* Journal of Biological Chemistry, 2008. **283**(51): p. 35724-35734.
48. Purvis, J.E., et al., *p53 dynamics control cell fate.* Science (New York, N.Y.), 2012. **336**(6087): p. 1440-1444.
49. Johnson, H.E., S.Y. Shvartsman, and J.E. Toettcher, *Signaling dynamics control cell fate in the early Drosophila embryo.* bioRxiv, 2018.
50. Behar, M. and A. Hoffmann, *Understanding the temporal codes of intra-cellular signals.* Current opinion in genetics & development, 2010. **20**(6): p. 684-693.
51. Purvis, Jeremy E. and G. Lahav, *Encoding and Decoding Cellular Information through Signaling Dynamics.* Cell, 2013. **152**(5): p. 945-956.
52. Ganesan, A. and J. Zhang, *How cells process information: quantification of spatiotemporal signaling dynamics.* Protein science : a publication of the Protein Society, 2012. **21**(7): p. 918-928.
53. Stephens, T.J., et al., *Progressive increase in human skeletal muscle AMPKα2 activity and ACC phosphorylation during exercise.* American Journal of Physiology-Endocrinology and Metabolism, 2002. **282**(3): p. E688-E694.
54. Gibala, M.J., et al., *Brief intense interval exercise activates AMPK and p38 MAPK signaling and increases the expression of PGC-1α in human skeletal muscle.* Journal of Applied Physiology, 2009. **106**(3): p. 929-934.
55. Fujii, N., et al., *Exercise Induces Isoform-Specific Increase in 5'AMP-Activated Protein Kinase Activity in Human Skeletal Muscle.* Biochemical and Biophysical Research Communications, 2000. **273**(3): p. 1150-1155.
56. Sriwijitkamol, A., et al., *Effect of Acute Exercise on AMPK Signaling in Skeletal Muscle of Subjects With Type 2 Diabetes.* A Time-Course and Dose-Response Study, 2007. **56**(3): p. 836-848.

57. Rose, A.J., et al., *Exercise rapidly increases eukaryotic elongation factor 2 phosphorylation in skeletal muscle of men.* The Journal of physiology, 2005. **569**(Pt 1): p. 223-228.
58. Wojtaszewski, J.F.P., et al., *Isoform-specific and exercise intensity-dependent activation of 5'-AMP-activated protein kinase in human skeletal muscle.* The Journal of Physiology, 2000. **528**(1): p. 221-226.
59. Wang, T., et al., *Exercise improves glucose uptake in murine myotubes through the AMPKα2-mediated induction of Sestrins.* Biochimica et Biophysica Acta (BBA) - Molecular Basis of Disease, 2018. **1864**(10): p. 3368-3377.
60. Nedachi, T., Fujita, H, and Kanzaki, M., *Contractile C2C12 myotube model for studying exercise-inducible responses in skeletal muscle.* American Journal of Physiology-Endocrinology and Metabolism, 2008. **295**(5): p. E1191-E1204.
61. Manabe, Y., et al., *Characterization of an Acute Muscle Contraction Model Using Cultured C2C12 Myotubes.* Plos One, 2012. **7**(12).
62. Li, Z., Yue, Y., Hu, F., Zhang, C., Ma, X., Li, N., Qiu, L., Fu, M., Chen, L., Yao, Z., Bilan, P. J., Klip, A., Niu, W., *Electrical pulse stimulation induces GLUT4 translocation in C2C12 myotubes that depends on Rab8A, Rab13, and Rab14.* American Journal of Physiology-Endocrinology and Metabolism, 2017. **314**(5): p. E478-E493.
63. Damschroder, D., et al., *Drosophila Endurance Training and Assessment of Its Effects on Systemic Adaptations.* Bio-protocol, 2018. **8**(19): p. e3037.
64. Laranjeiro, R., et al., *Single swim sessions in C. elegans induce key features of mammalian exercise.* BMC Biology, 2017. **15**(1): p. 30.
65. Colquitt, R.B., D.A. Colquhoun, and R.H. Thiele, *In silico modelling of physiologic systems.* Best Practice & Research Clinical Anaesthesiology, 2011. **25**(4): p. 499-510.
66. del Carmen Ortuño-Costela, M., et al., *iPSCs: A powerful tool for skeletal muscle tissue engineering.* Journal of Cellular and Molecular Medicine, 2019. **23**(6): p. 3784-3794.
67. Gholobova, D., et al., *Human tissue-engineered skeletal muscle: a novel 3D in vitro model for drug disposition and toxicity after intramuscular injection.* Scientific Reports, 2018. **8**(1): p. 12206.
68. Khodabukus, A., et al., *In Vitro Tissue-Engineered Skeletal Muscle Models for Studying Muscle Physiology and Disease.* Advanced healthcare materials, 2018. **7**(15): p. e1701498-e1701498.
69. Mertens, J.P., et al., *Engineering muscle constructs for the creation of functional engineered musculoskeletal tissue.* Regenerative medicine, 2014. **9**(1): p. 89-100.
70. Nikolić, N., et al., *Electrical pulse stimulation of cultured skeletal muscle cells as a model for in vitro exercise – possibilities and limitations.* Acta Physiologica, 2017. **220**(3): p. 310-331.
71. Nikolić, N., et al., *Electrical Pulse Stimulation of Cultured Human Skeletal Muscle Cells as an In Vitro Model of Exercise.* PLOS ONE, 2012. **7**(3): p. e33203.
72. Carter, S. and T.P.J. Solomon, *In vitro experimental models for examining the skeletal muscle cell biology of exercise: the possibilities, challenges and future developments.* Pflügers Archiv - European Journal of Physiology, 2019. **471**(3): p. 413-429.
73. Shainberg, A. and M. Burstein, *Decrease of acetylcholine receptor synthesis in muscle cultures by electrical stimulation.* Nature, 1976. **264**(5584): p. 368-369.
74. Orfanos, Z., et al., *Breaking sarcomeres by in vitro exercise.* Scientific Reports, 2016. **6**: p. 19614.

75. Yaffe, D. and O. Saxel, *Serial passaging and differentiation of myogenic cells isolated from dystrophic mouse muscle.* Nature, 1977. **270**(5639): p. 725.
76. Veliça, P. and C.M. Bunce, *A quick, simple and unbiased method to quantify C2C12 myogenic differentiation.* Muscle & Nerve, 2011. **44**(3): p. 366-370.
77. Yoshiko, Y., K. Hirao, and N. Maeda, *Differentiation in C2C12 myoblasts depends on the expression of endogenous IGFs and not serum depletion.* American Journal of Physiology-Cell Physiology, 2002. **283**(4): p. C1278-C1286.
78. McMahon, D.K., et al., *C2C12 cells: biophysical, biochemical, and immunocytochemical properties.* American Journal of Physiology-Cell Physiology, 1994. **266**(6): p. C1795-C1802.
79. Liang, R., et al., *Modeling Myotonic Dystrophy 1 in C2C12 Myoblast Cells.* Journal of visualized experiments : JoVE, 2016(113): p. 54078.
80. Fujita, H., T. Nedachi, and M. Kanzaki, *Accelerated de novo sarcomere assembly by electric pulse stimulation in C2C12 myotubes.* Experimental Cell Research, 2007. **313**(9): p. 1853-1865.
81. Egan, B. and Juleen R. Zierath, *Exercise Metabolism and the Molecular Regulation of Skeletal Muscle Adaptation.* Cell Metabolism, 2013. **17**(2): p. 162-184.
82. Son, Y.H., et al., *Comparative molecular analysis of endurance exercise in vivo with electrically stimulated in vitro myotube contraction.* Journal of Applied Physiology, 2019. **127**(6): p. 1742-1753.
83. Liu, C.-T. and G.A. Brooks, *Mild heat stress induces mitochondrial biogenesis in C2C12 myotubes.* Journal of applied physiology (Bethesda, Md. : 1985), 2012. **112**(3): p. 354-361.
84. Lindholm, M.E. and H. Rundqvist, *Skeletal muscle hypoxia-inducible factor-1 and exercise.* Experimental Physiology, 2016. **101**(1): p. 28-32.
85. Chen, R., et al., *Effects of cobalt chloride, a hypoxia-mimetic agent, on autophagy and atrophy in skeletal C2C12 myotubes.* BioMed research international, 2017. **2017**.
86. Berggren, J.R., C.J. Tanner, and J.A. Houmard, *Primary cell cultures in the study of human muscle metabolism.* Exercise and sport sciences reviews, 2007. **35**(2): p. 56-61.
87. Tarum, J., et al., *Electrical pulse stimulation: an in vitro exercise model for the induction of human skeletal muscle cell hypertrophy. A proof-of-concept study.* Experimental Physiology, 2017. **102**(11): p. 1405-1413.
88. Stuart, J.A., et al., *How Supraphysiological Oxygen Levels in Standard Cell Culture Affect Oxygen-Consuming Reactions.* Oxidative Medicine and Cellular Longevity, 2018. **2018**: p. 13.
89. Carreau, A., et al., *Why is the partial oxygen pressure of human tissues a crucial parameter? Small molecules and hypoxia.* Journal of Cellular and Molecular Medicine, 2011. **15**(6): p. 1239-1253.
90. Airley, R.E. and A. Mobasheri, *Hypoxic Regulation of Glucose Transport, Anaerobic Metabolism and Angiogenesis in Cancer: Novel Pathways and Targets for Anticancer Therapeutics.* Chemotherapy, 2007. **53**(4): p. 233-256.
91. Wei, Y., et al., *Review of Dissolved Oxygen Detection Technology: From Laboratory Analysis to Online Intelligent Detection.* Sensors (Basel, Switzerland), 2019. **19**(18): p. 3995.
92. Carpenter, J.H., *The accuracy of the winkler method for dissolved oxygen analysis.* Limnology and Oceanography, 1965. **10**(1): p. 135-140.
93. Amao, Y., *Probes and Polymers for Optical Sensing of Oxygen.* Microchimica Acta, 2003. **143**(1): p. 1-12.

94. Vanderkooi, J.M., et al., *An optical method for measurement of dioxygen concentration based upon quenching of phosphorescence.* Journal of Biological Chemistry, 1987. **262**(12): p. 5476-5482.
95. Korthuis, R., *Skeletal Muscle Circulation. San Rafael (CA): Morgan & Claypool Life Sciences; 2011. Chapter 4, Exercise Hyperemia and Regulation of Tissue Oxygenation During Muscular Activity*. 2011.
96. Bontemps, F., G. Van den Berghe, and H.G. Hers, *Pathways of adenine nucleotide catabolism in erythrocytes.* The Journal of Clinical Investigation, 1986. **77**(3): p. 824-830.
97. Kim, J., et al., *AMPK activators: mechanisms of action and physiological activities.* Experimental & Molecular Medicine, 2016. **48**(4): p. e224-e224.
98. Corton, J.M., et al., *5-Aminoimidazole-4-Carboxamide Ribonucleoside.* European Journal of Biochemistry, 1995. **229**(2): p. 558-565.
99. Young, M.E., G.K. Radda, and B. Leighton, *Activation of glycogen phosphorylase and glycogenolysis in rat skeletal muscle by AICAR — an activator of AMP-activated protein kinase.* FEBS Letters, 1996. **382**(1): p. 43-47.
100. Narkar, V.A., et al., *AMPK and PPARdelta Agonists Are Exercise Mimetics.* Cell, 2008. **134**(3): p. 405-415.
101. Vincent, M.F., et al., *Inhibition by AICA Riboside of Gluconeogenesis in Isolated Rat Hepatocytes.* Diabetes, 1991. **40**(10): p. 1259-1266.
102. Göransson, O., et al., *Mechanism of action of A-769662, a valuable tool for activation of AMP-activated protein kinase.* The Journal of biological chemistry, 2007. **282**(45): p. 32549-32560.
103. Cool, B., et al., *Identification and characterization of a small molecule AMPK activator that treats key components of type 2 diabetes and the metabolic syndrome.* Cell Metabolism, 2006. **3**(6): p. 403-416.
104. Sanders, M.J., et al., *Defining the mechanism of activation of AMP-activated protein kinase by the small molecule A-769662, a member of the thienopyridone family.* Journal of biological chemistry, 2007. **282**(45): p. 32539-32548.
105. Scott, J.W., et al., *Thienopyridone Drugs Are Selective Activators of AMP-Activated Protein Kinase β1-Containing Complexes.* Chemistry & Biology, 2008. **15**(11): p. 1220-1230.
106. Vincent, E.E., et al., *Differential effects of AMPK agonists on cell growth and metabolism.* Oncogene, 2015. **34**(28): p. 3627-3639.
107. Sinnett, S.E. and J.E. Brenman, *Past strategies and future directions for identifying AMP-activated protein kinase (AMPK) modulators.* Pharmacology & therapeutics, 2014. **143**(1): p. 111-118.
108. Zhou, G., et al., *Role of AMP-activated protein kinase in mechanism of metformin action.* The Journal of clinical investigation, 2001. **108**(8): p. 1167-1174.
109. Dite, T.A., et al., *AMP-activated protein kinase selectively inhibited by the type II inhibitor SBI-0206965.* Journal of Biological Chemistry, 2018. **293**(23): p. 8874-8885.
110. Handa, N., et al., *Structural basis for compound C inhibition of the human AMP-activated protein kinase α2 subunit kinase domain.* Acta Crystallographica Section D, 2011. **67**(5): p. 480-487.
111. Bain, J., et al., *The selectivity of protein kinase inhibitors: a further update.* The Biochemical journal, 2007. **408**(3): p. 297-315.
112. Van Der Putten, W.J.M. and J.M. Kelly, *Laser flash spectroscopy of methylene blue with nucleic acids. Effects of ionic strength and pH.* Photochemistry and Photobiology, 1989. **49**(2): p. 145-151.

113. Waheed, A.A., K.S. Rao, and P.D. Gupta, *Mechanism of Dye Binding in the Protein Assay Using Eosin Dyes.* Analytical Biochemistry, 2000. **287**(1): p. 73-79.
114. Schneider, C.A., W.S. Rasband, and K.W. Eliceiri, *NIH Image to ImageJ: 25 years of image analysis.* Nature methods, 2012. **9**(7): p. 671.
115. Munday, M.R., et al., *Identification by amino acid sequencing of three major regulatory phosphorylation sites on rat acetyl-CoA carboxylase.* European Journal of Biochemistry, 1988. **175**(2): p. 331-338.
116. Taylor, E.B., et al., *Discovery of TBC1D1 as an Insulin-, AICAR-, and Contraction-stimulated Signaling Nexus in Mouse Skeletal Muscle.* Journal of Biological Chemistry, 2008. **283**(15): p. 9787-9796.
117. Ladner, C.L., et al., *Visible fluorescent detection of proteins in polyacrylamide gels without staining.* Analytical Biochemistry, 2004. **326**(1): p. 13-20.
118. Grishagin, I.V., *Automatic cell counting with ImageJ.* Analytical Biochemistry, 2015. **473**: p. 63-65.
119. Team, R., *RStudio: integrated development for R.* RStudio, Inc., Boston, MA URL http://www. rstudio. com, 2015. **42**: p. 14.
120. Bates, D., et al., *Fitting linear mixed-effects models using lme4.* arXiv preprint arXiv:1406.5823, 2014.
121. Korzeniewski, C. and D.M. Callewaert, *An enzyme-release assay for natural cytotoxicity.* Journal of Immunological Methods, 1983. **64**(3): p. 313-320.
122. Denes, L.T., et al., *Culturing C2C12 myotubes on micromolded gelatin hydrogels accelerates myotube maturation.* Skeletal Muscle, 2019. **9**(1): p. 17.
123. Nieuwoudt, S., et al., *In vitro contraction protects against palmitate-induced insulin resistance in C2C12 myotubes.* American Journal of Physiology-Cell Physiology, 2017. **313**(5): p. C575-C583.
124. Abdelmoez, A.M., et al., *Comparative profiling of skeletal muscle models reveals heterogeneity of transcriptome and metabolism.* American Journal of Physiology-Cell Physiology, 2020. **318**(3): p. C615-C626.
125. Robinson, M.M., et al., *Robust intrinsic differences in mitochondrial respiration and H2O2 emission between L6 and C2C12 cells.* Am J Physiol Cell Physiol, 2019.
126. Marsin, A.S., et al., *Phosphorylation and activation of heart PFK-2 by AMPK has a role in the stimulation of glycolysis during ischaemia.* Current Biology, 2000. **10**(20): p. 1247-1255.
127. Sanchis-Gomar, F., et al., *Neuromuscular Electrical Stimulation: A New Therapeutic Option for Chronic Diseases Based on Contraction-Induced Myokine Secretion.* Frontiers in Physiology, 2019. **10**(1463).
128. Salmons, S., *Adaptive change in electrically stimulated muscle: A framework for the design of clinical protocols.* Muscle & Nerve, 2009. **40**(6): p. 918-935.
129. Doucet, B.M., A. Lam, and L. Griffin, *Neuromuscular electrical stimulation for skeletal muscle function.* The Yale journal of biology and medicine, 2012. **85**(2): p. 201-215.
130. Brown, D.I., M.S. Willis, and J.M. Berthiaume, *Chapter 11 - Influence of Ischemia-Reperfusion Injury on Cardiac Metabolism*, in *The Scientist's Guide to Cardiac Metabolism*, M. Schwarzer and T. Doenst, Editors. 2016, Academic Press: Boston. p. 155-167.
131. Chisholm, G. and L. Cronin, *Chapter 16 - Hydrogen From Water Electrolysis*, in *Storing Energy*, T.M. Letcher, Editor. 2016, Elsevier: Oxford. p. 315-343.
132. Da Boit, M., et al., *Sex differences in the response to resistance exercise training in older people.* Physiological reports, 2016. **4**(12): p. e12834.

133. Timmons, J.A., *Variability in training-induced skeletal muscle adaptation.* Journal of Applied Physiology, 2010. **110**(3): p. 846-853.

Appendix

Please see the attached appendix files for the following resources (Appendix 1 – 11 are in the 'Appendix.xlsl' file):

Appendix 1:	Product Information
Appendix 2:	Western Blot Protocol
Appendix 3:	Lysis Protocol
Appendix 4:	Buffer Recipes
Appendix 5:	Lysis Buffer Recipes
Appendix 6:	BCA Protocol
Appendix 7:	Lambda-Phosphatase Protocol
Appendix 8:	[ATP]i Protocol
Appendix 9:	LDH Protocol
Appendix 10:	L-lactate Protocol
Appendix 11:	Lucid O_2 Probe Calibration Protocol
Appendix_RCode.R	R code required to re-create statistical analyses and figures presented in this thesis